Cosmological constraints from the abundance of galaxy clusters in the *eROSITA All-Sky Survey*

Nicolas Clerc
IRAP (CNRS/UPS/CNES) Toulouse

LPNHE Seminar
24 June 2024

First eROSITA all-sky survey cosmology results

Ghirardini et al. (2024) – Astronomy & Astrophysics in press.

Grandis et al. (2024) ; Seppi et al. (2024), Clerc et al. (2024), Kleinebreil et al. (2024), Liu et al. (2024), Artis et al. (2024)

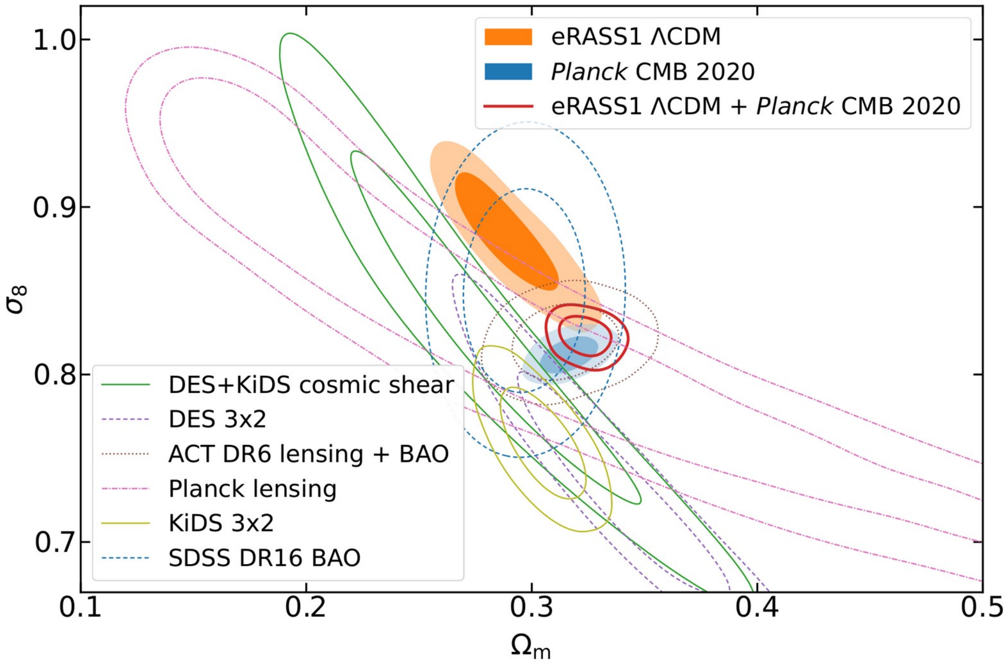

Merloni et al. (2024) – Astronomy & Astrophysics

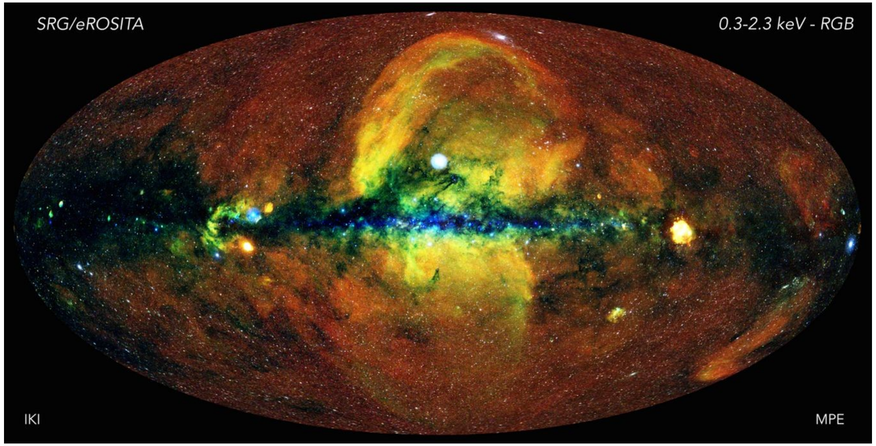

Bulbul et al. (2024) – Astronomy & Astrophysics ; Kluge et al. A&A in press.

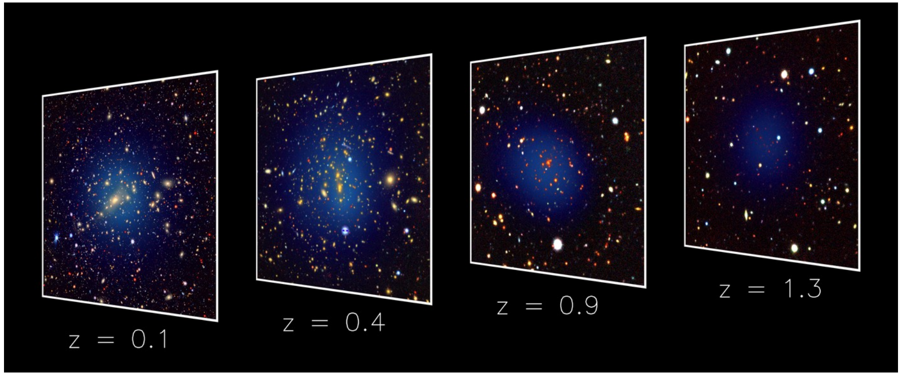

Outline

1. Cosmological constraints from X-ray galaxy cluster surveys
2. The *eROSITA* All-Sky Survey
3. Cosmology results from eRASS1 clusters
4. Perspectives

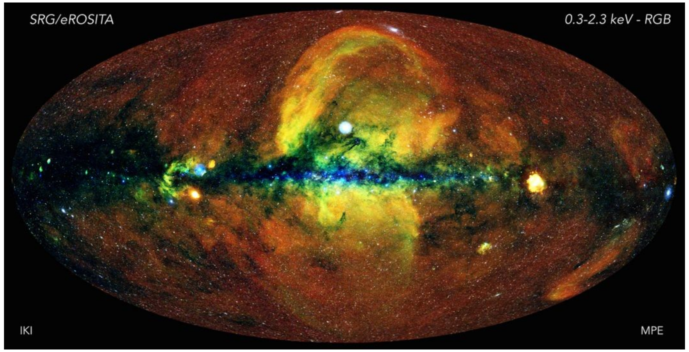

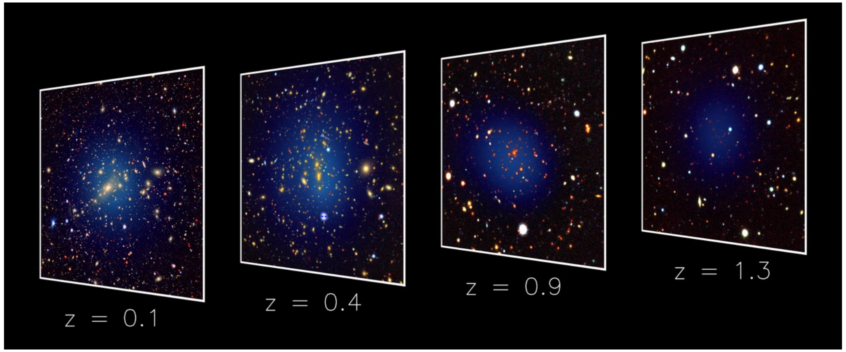

Galaxy clusters as cosmological probes

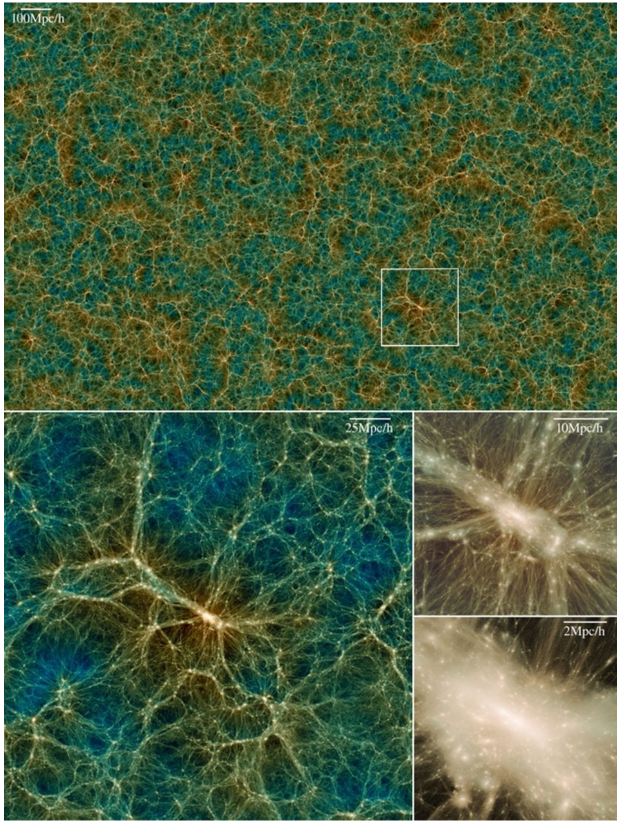

Uchuu simulations (Ishiyama et al. 2021)

The distribution of matter halos is a robust prediction of (CDM) cosmological models

Galaxy clusters are the most massive (~$10^{14\text{-}15}$ M_{sol}) bound structures, latest to form in an expanding Universe. Made of 85% dark matter, 12% hot gas, 3% galaxies

The hot intracluster gas trapped in massive halos emits copious amounts of X-ray photons tracing total mass

The halo mass function is a cosmological observable

$$\frac{\mathrm{d}n}{\mathrm{d}M}(M,z) = f(\sigma)\frac{\rho_b}{M^2}\frac{\mathrm{d}\ln\sigma^{-1}}{\ln M}$$

$$\sigma^2(R,z) = \frac{1}{2\pi}\int P_L(k,z)|\hat{W}_R(k)|^2 k^2 \mathrm{d}k$$

→ variance of the smoothed linear matter density field

$$P_L(k,z) \propto D_+^2(z) T^2(k) k^{n_s}$$

→ involves linear growth factor and matter transfer function

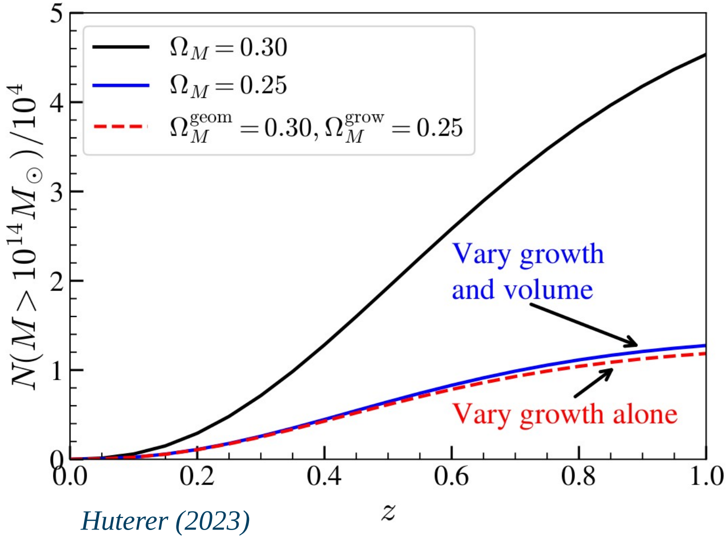

Huterer (2023)

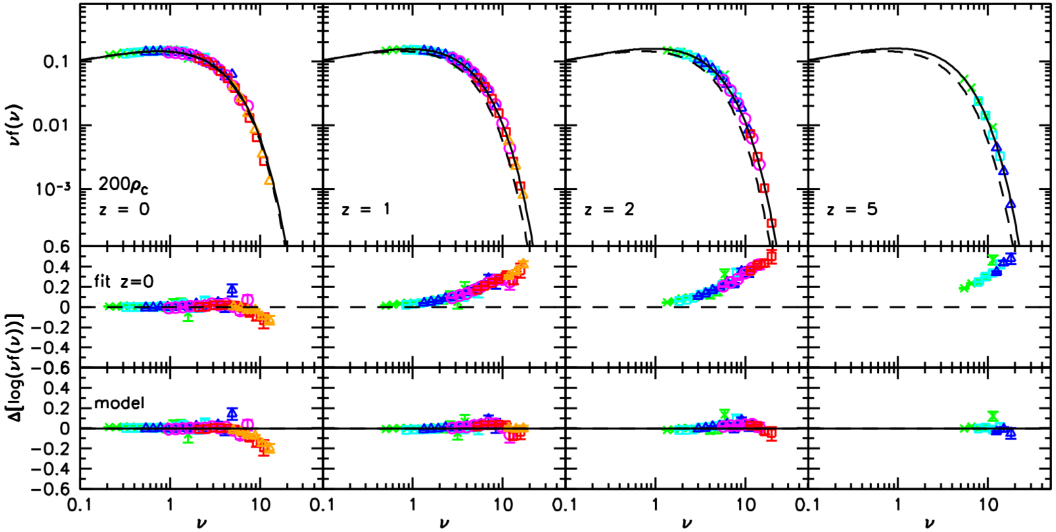

Despali et al. (2016)

The halo mass function is a cosmological observable

Vikhlinin et al. (2009)

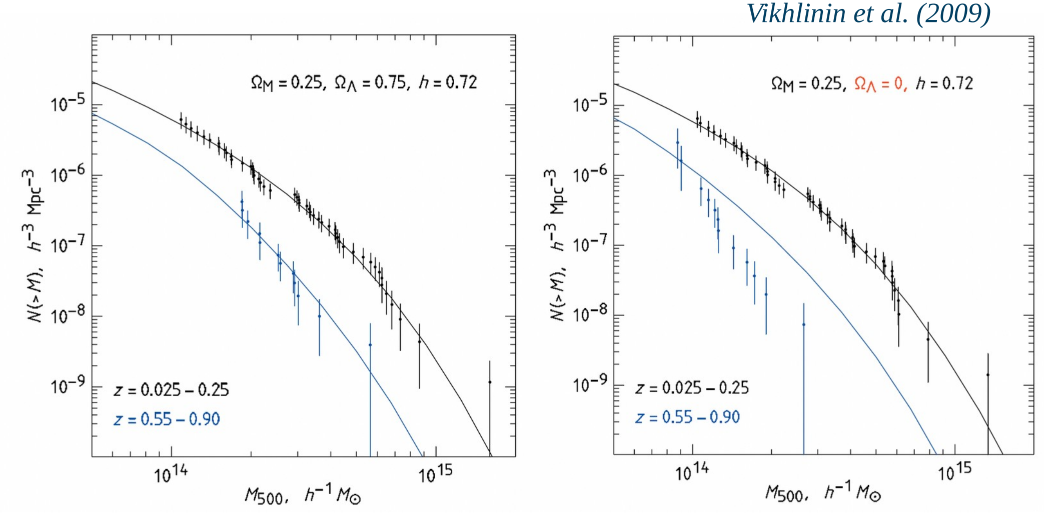

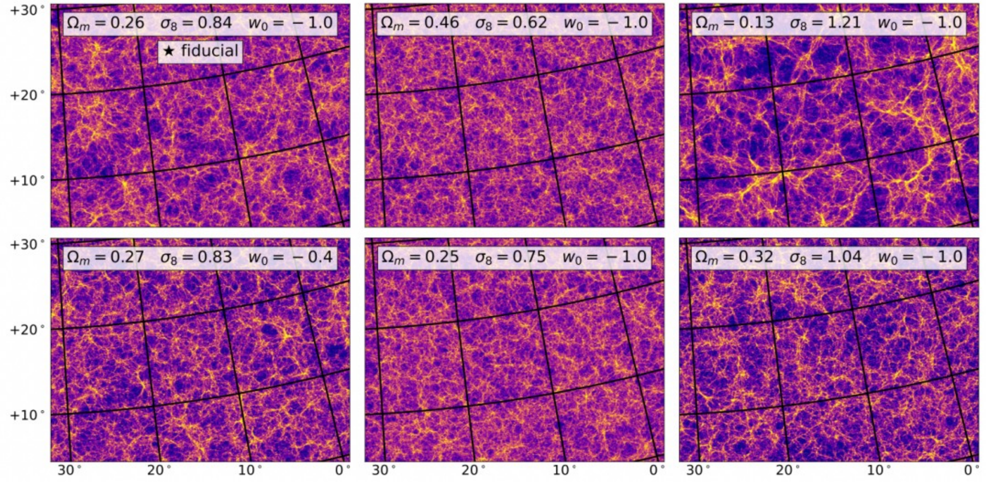

Kacprzac et al. (2023)

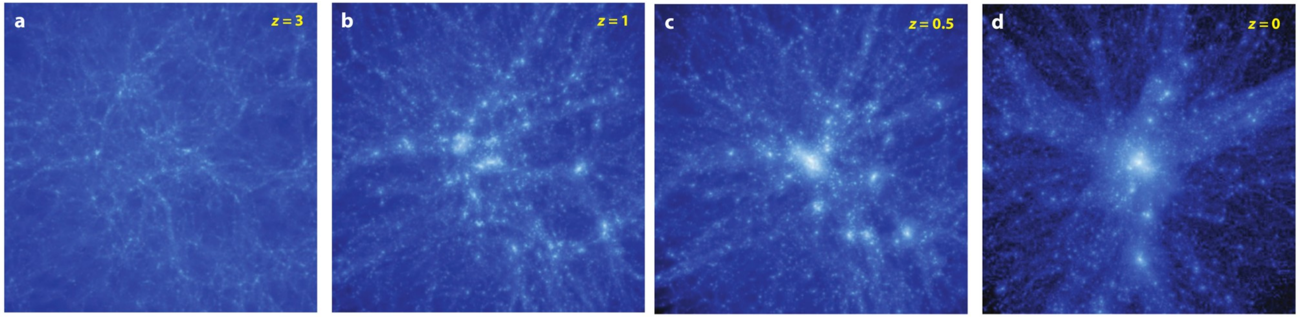

Kravtsov & Borgani 2012

Tight link between mass and intracluster gas observables

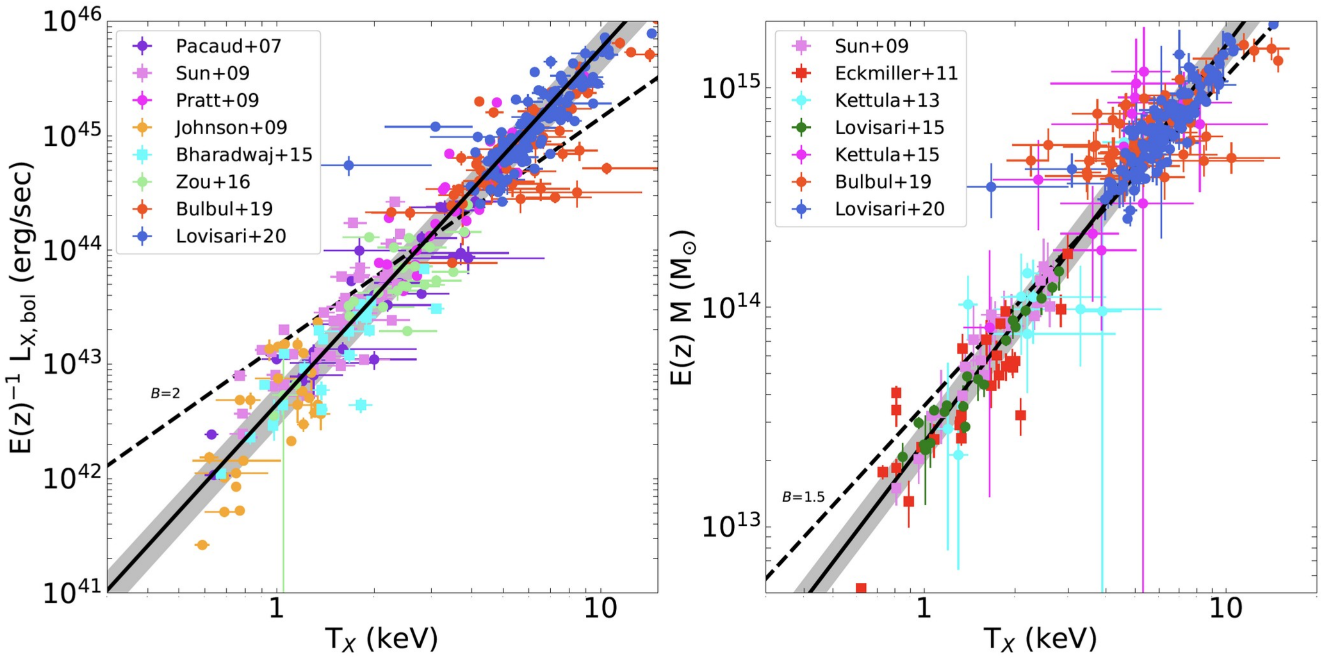

Lovisari & Maughan (2023)

- **The relation between total mass and observables (luminosity, temperature, gas mass, etc.) is well-established observationally and theoretically**
  - This is the current systematic limit in cosmology analyses

- **Major developments in the last ~10 years involve support from gravitational lensing to calibrate the gas observables**
  + Deep astrophysical observations to understand scatter and bias

A variety of cosmological tests with clusters

Besides the halo mass function, multiple tests utilize clusters to constrain cosmology

- Spatial distribution in 3D space of clusters and groups
- “Standard candles” through the constant baryon fraction budget of clusters (~ closed boxes)
- Matter profiles and evolution to constrain the growth of large-scale structures
- Searching for extreme objects in mass/velocity/redshift space to rule out cosmological models
- H_0 from cluster 3-dimensional shapes, etc.

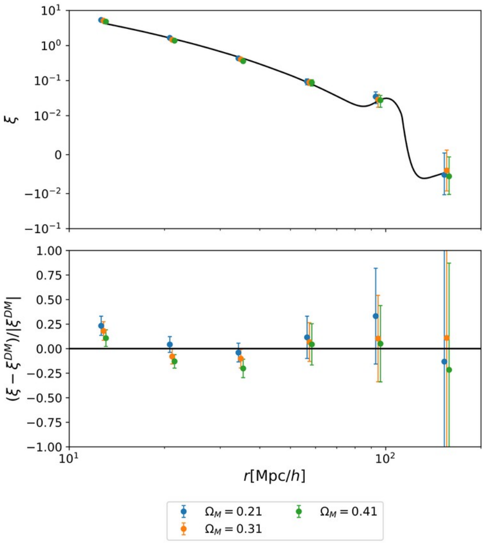

Lindholm et al. (2021)

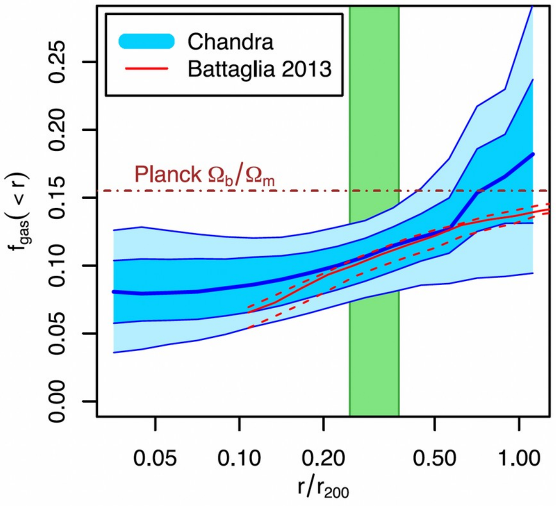

Mantz et al. (2014)

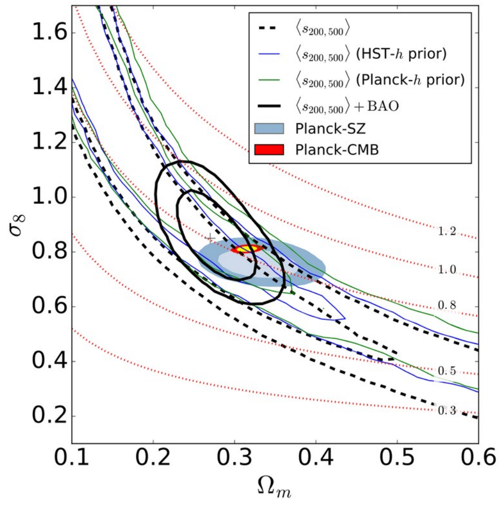

Corasaniti et al. (2021)

Abundance constraints require large X-ray surveys

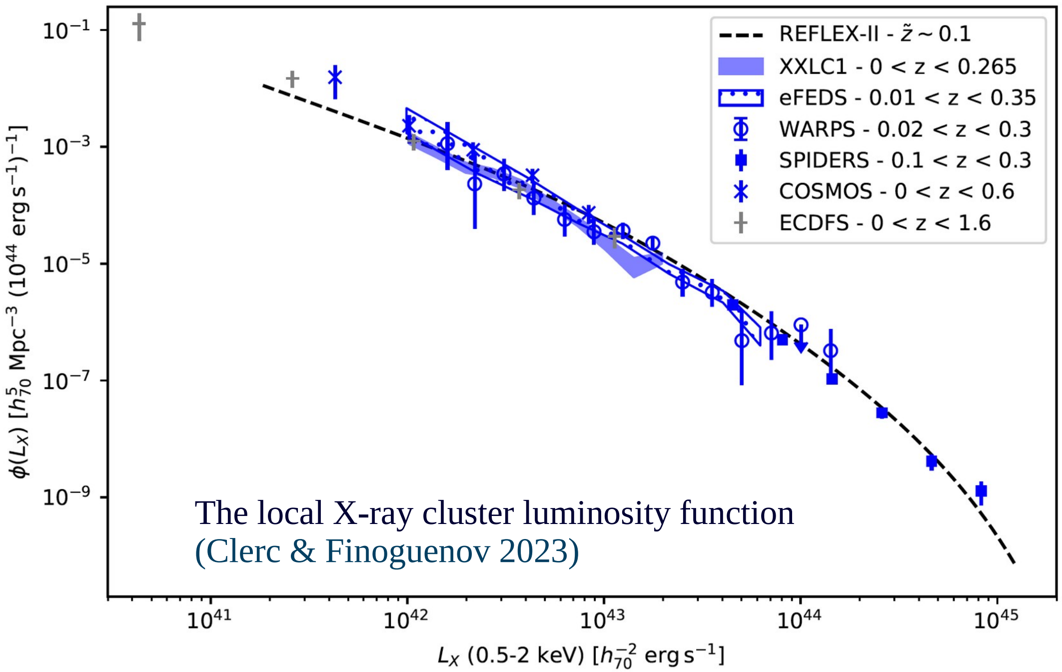

- **Galaxy clusters are rare entities**
- **Most massive are most constraining**
- **Cataloging small-mass systems is required to understand the observable-mass relation**

- Large survey → large Universe volumes
- High sensitivity → large mass range
- Angular resolution → disambiguation
- Optical follow-up → redshift, distance

eROSITA onboard SRG

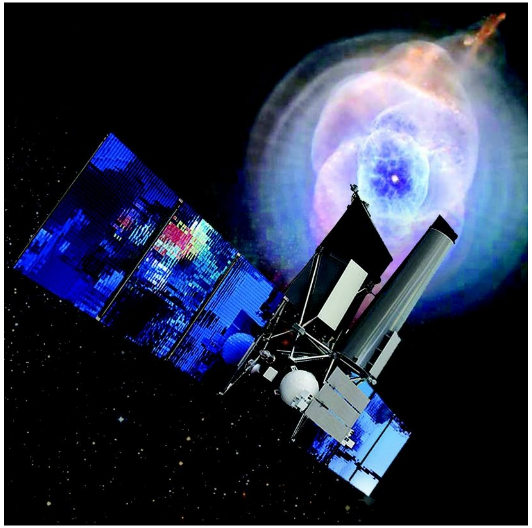

eROSITA = extended ROetgen Survey with an Imaging Telescope Array
It is the primary instrument onboard the SRG observatory.
An X-ray telescope optimised for X-ray surveys.

Spektr-RG (SRG) is a joint mission between Russian and German institutes and agencies
eROSITA is the German contribution to the mission (PI: MPE Garching)

Source: Roscosmos/DLR/SRG/Lavochkin

eROSITA onboard SRG

The eROSITA all-sky surveys

- **Launch from Baikonour to L2 on 13/7/2019**
- 3 months flight to L2: verification & calibration
- 6 months ↔ 1 full-sky coverage
- Data shared MPE (Germany) / IKI (Russia)

- **One "eROday" = 4 hours = 1 great circle**
- Each point of the sky visited multiple times
- X-ray photons accumulated to increase depth

Credits DLR

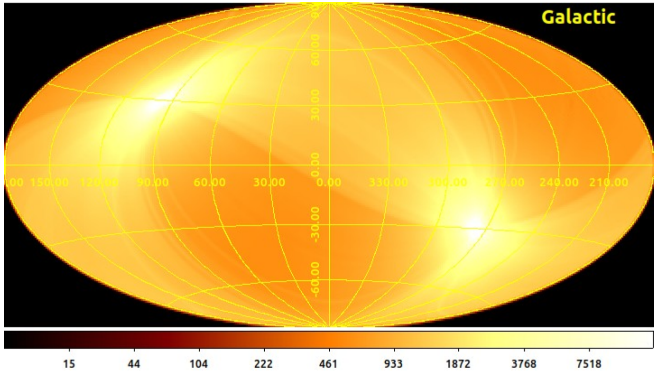

Credits Hamburg observatory

The eROSITA instrument – the telescope

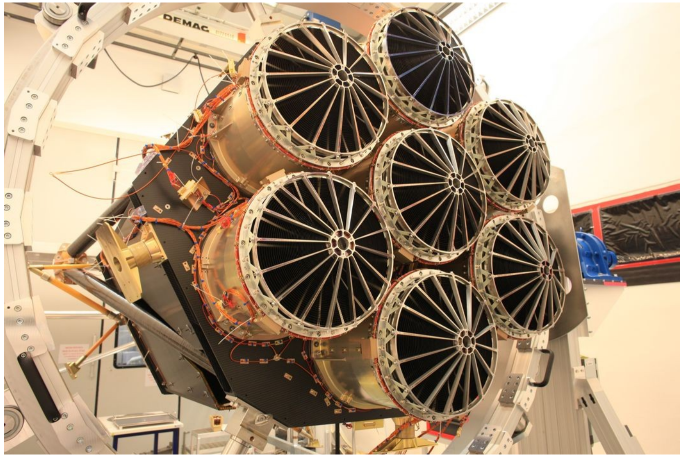

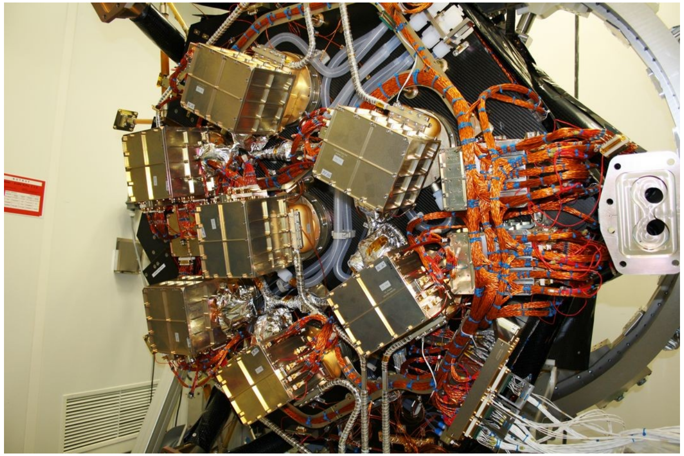

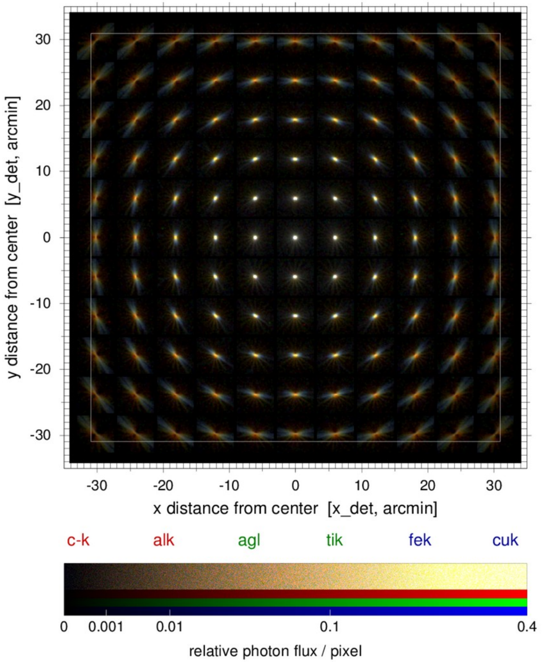

Predehl et al. (2021)

- Large Effective area (~1300 cm^2 @1 keV, ~*XMM-Newton*)
- Large Field of view: 1 degree (diameter)
- Half-Energy width (HEW) ~18” (on-axis, point.); ~30” (FoV avg., survey)
- Positional accuracy: ~4.5” (1σ)
- X-ray baffle: 92% stray light reduction
- Cameras: pnCCD with framestore: 384×384×7 ~ 10^6 pixels (9.4”), no chip gaps
- Spectral resolution at all measured energies within specs (~80 eV @ 1.5 keV)

The eROSITA instrument – a survey machine

Predehl et al. (2021)

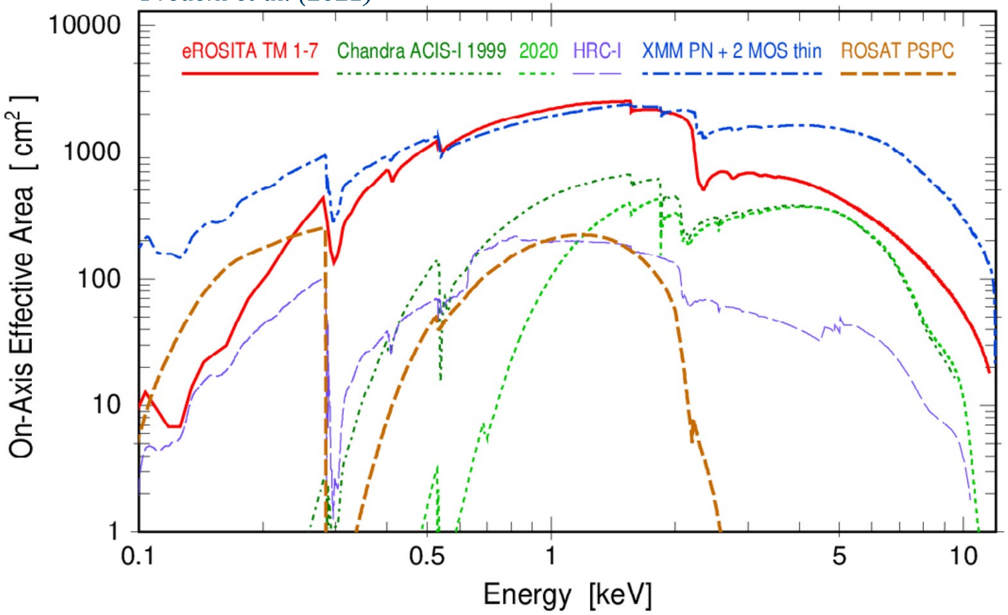

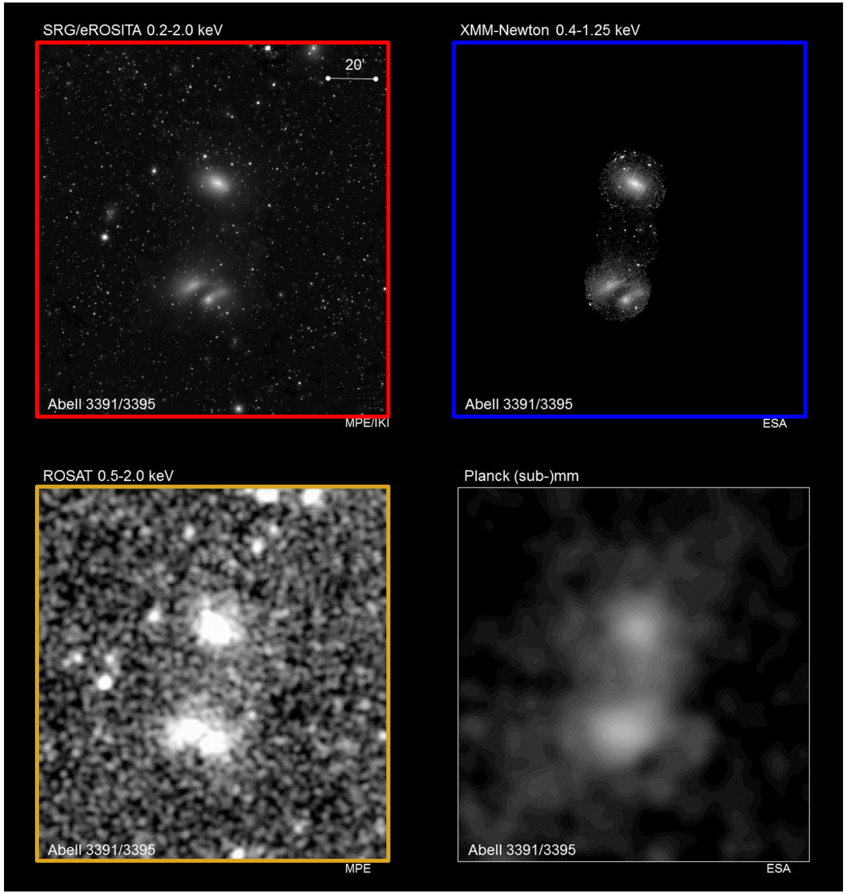

T. Reiprich (Univ. Bonn), M. Ramos-Ceja (MPE), F. Pacaud (Univ. Bonn), D. Eckert (Univ. Geneva), J. Sanders (MPE), N. Ota (Univ. Bonn), E. Bulbul (MPE), V. Ghirardini (MPE), J. Erler (Univ. Bonn), A. Veronica (Univ. Bonn)

The first eROSITA all-sky survey: eRASS1

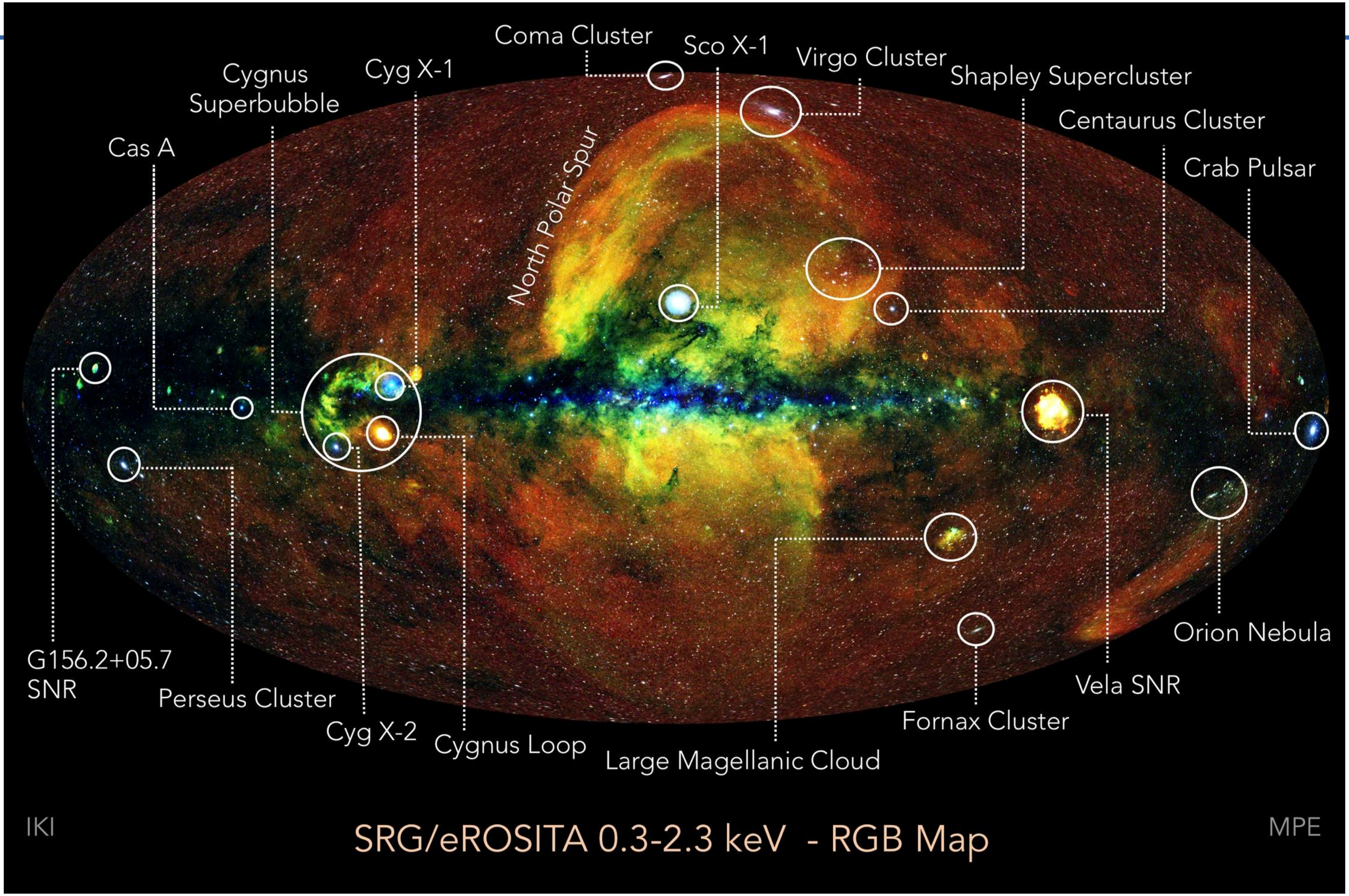

The eROSITA_DE consortium

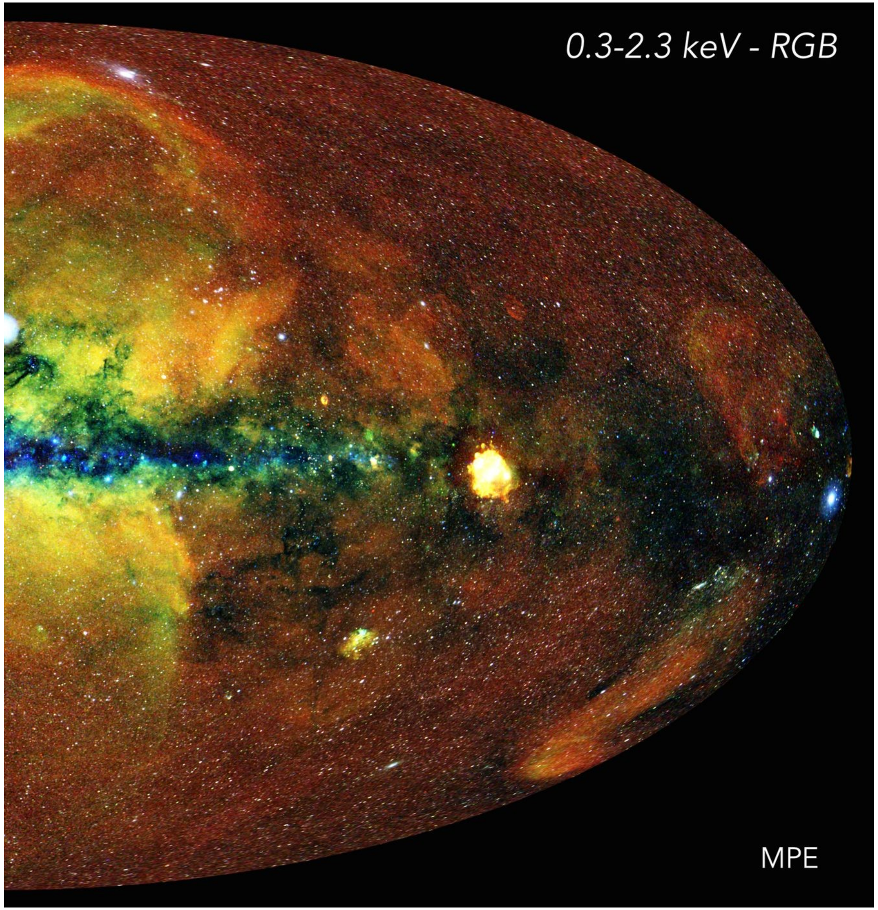

- **The German eROSITA_DE consortium**
  - Lead institute MPE (Garching)
  - Core institutes Uni. Hamburg, AIP (Potsdam), ECAP+Obs. Bamberg, IAA (Tübingen)
  - Participating institutes (Aifa Bonn, LMU)
- **12 working groups covering science and infrastructure activities**
  - Incl. Cosmology & clusters, AGN, stars, calibration, backgrounds, etc.
- **Responsible for the exploitation and release of the X-ray data under their responsibility**
  - Organised in terms of “Data Releases”: Early Data Release (incl. PV phase observations) and DR1.

The eROSITA_DE first data release (Jan. 31st 2024)

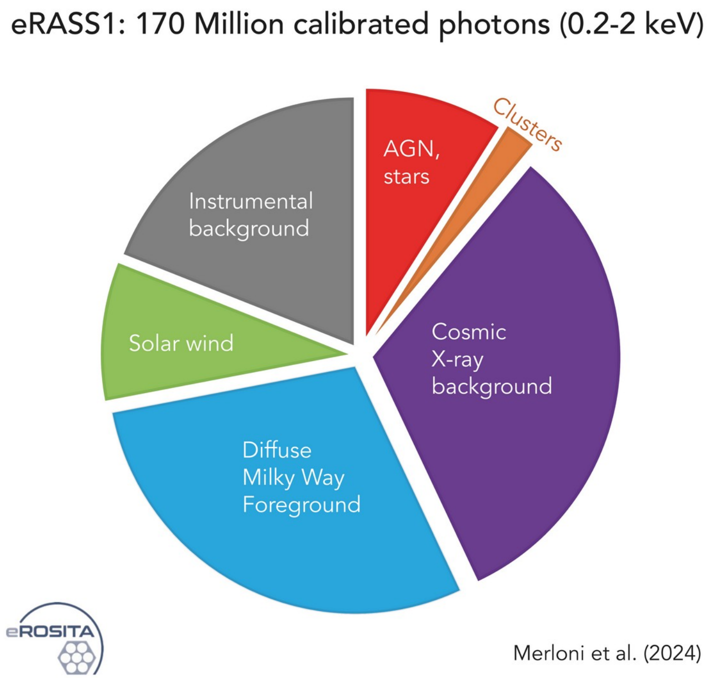

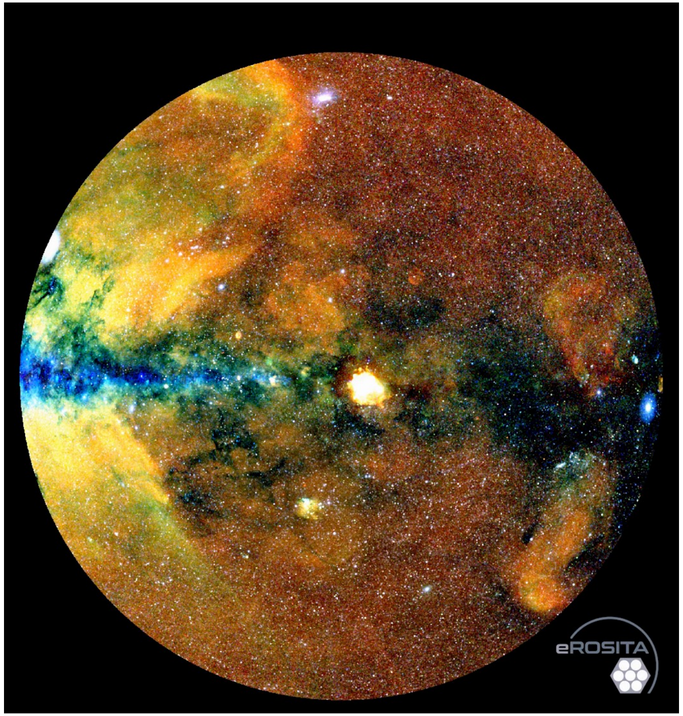

Merloni et al. (2024)

Content of the eRASS1 survey – point sources

- **0.9 million point sources: doubles the number of known X-ray sources!**

- Mostly active galactic nuclei (700k) and active stars (140k) + X-ray binaries, neutron stars, etc.

NOIRLab/NSF/AURA/J. da Silva

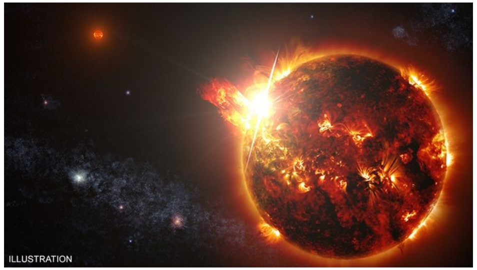

NASA/CXC/INAF/Argiroffi, C. et al.
Illustration: NASA/GSFC/S. Wiessinger

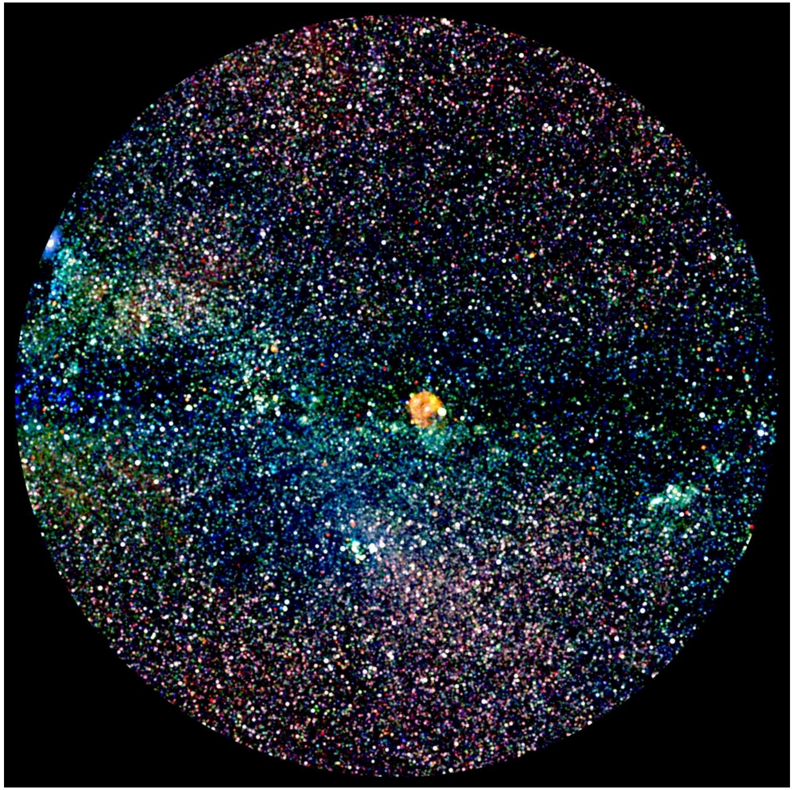

MPE, J. Sanders for the eROSITA consortium

Merloni et al. (2024)

Content of the eRASS1 survey – extended sources

- **Extended features include:**
- Galaxy clusters
- Supernova remnants
- Milky Way hot circum-galactic medium
- Local hot bubble
- Solar Wind Charge Exchange emission
- Cosmic X-ray background (AGN + SF galaxies)
- Intstrument backgrounds

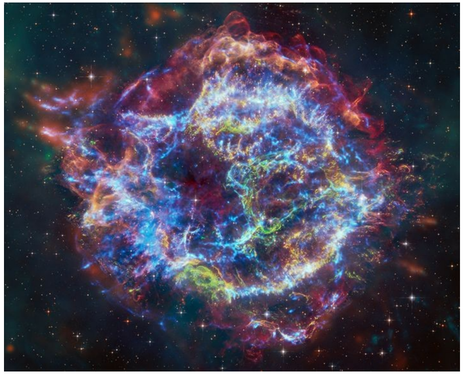

X-ray: NASA/CXC/SAO; Optical: NASA/ESA/STScI; IR: NASA/ESA/CSA/STScI/Milisavljevic et al., NASA/JPL/CalTech; Image Processing: NASA/CXC/SAO/J. Schmidt and K. Arcand

NASA/CXC/GSFC/S.A.Walker, et al.

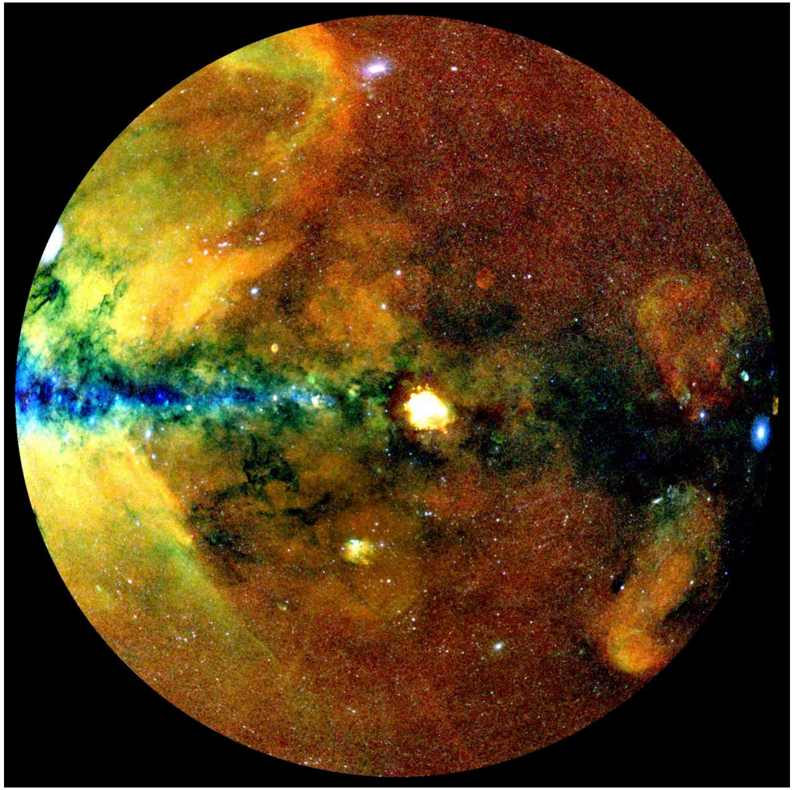

MPE, J. Sanders for the eROSITA consortium

Merloni et al. (2024)

The eRASS1 galaxy cluster catalog

- **12 247 X-ray detected, optically confirmed clusters** over 13 116 deg^2 sky area (Bulbul et al. 2024)
- **Optical photometric redshifts 0.003 < z < 1.32** with *grz* DESI Legacy Surveys (Kluge et al. 2024)
- **Gas distribution modeling from X-ray data** using a forward-modelling approach: fluxes, temperatures, gas mass, total mass

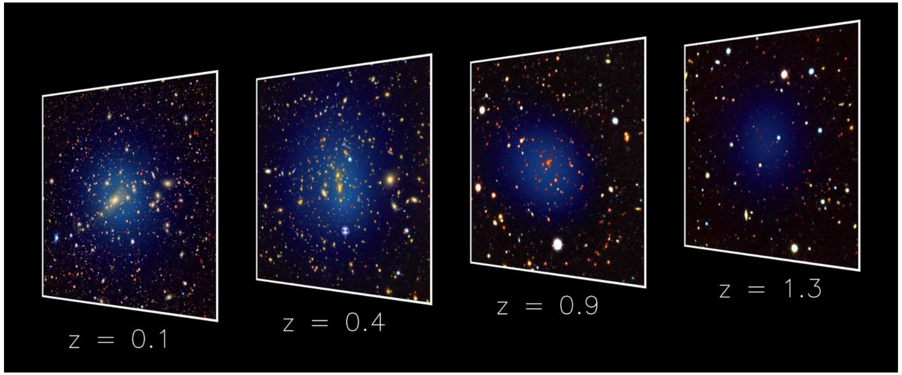

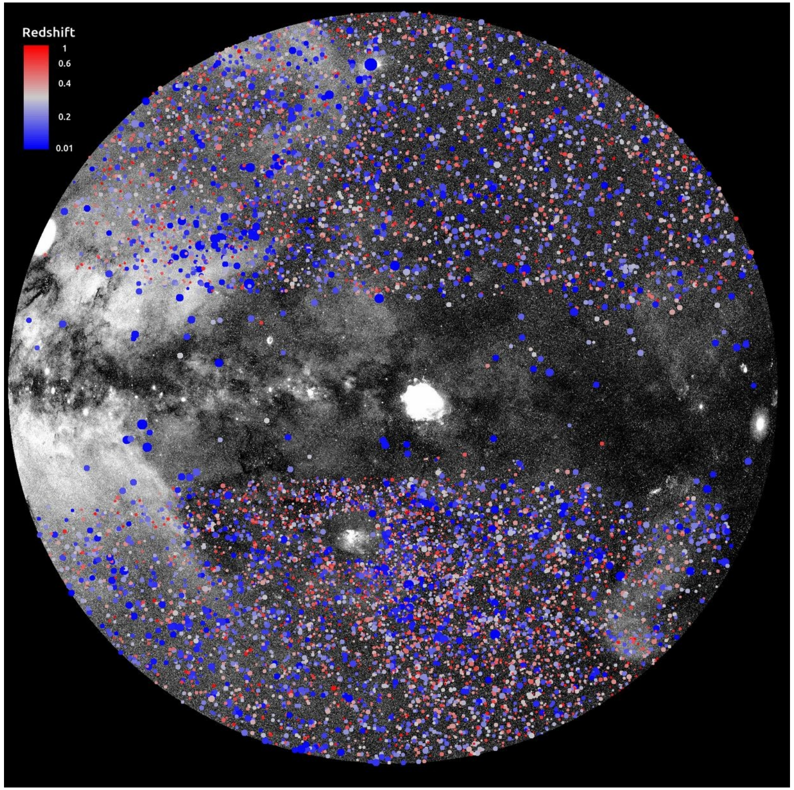

MPE, J. Sanders for the eROSITA consortium

The eRASS1 galaxy cluster catalog

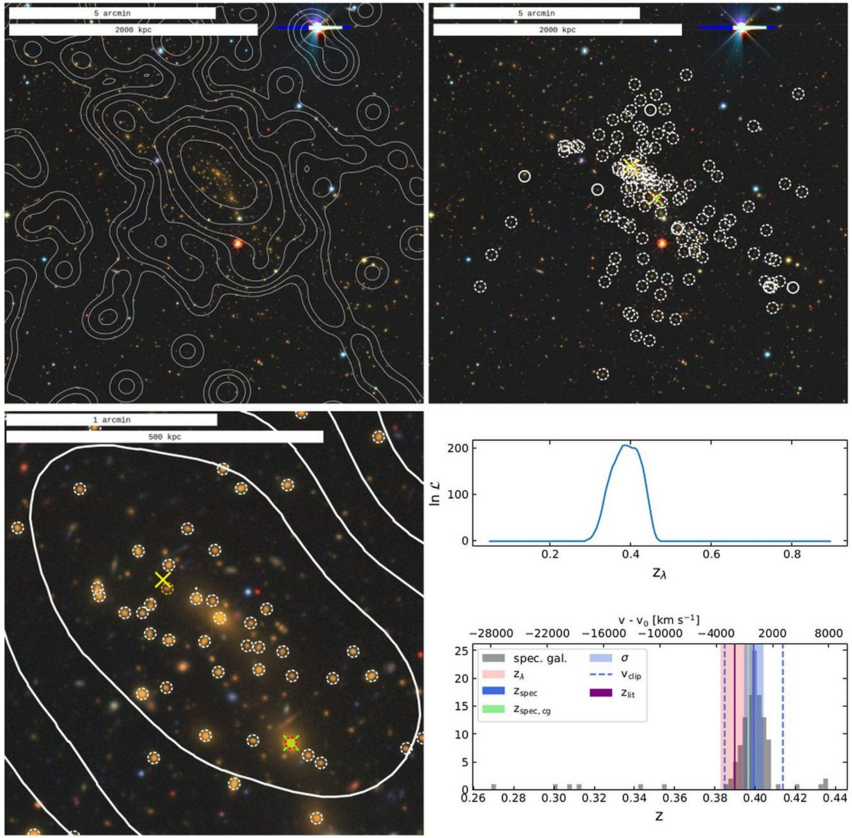

Kluge et al. (2024)

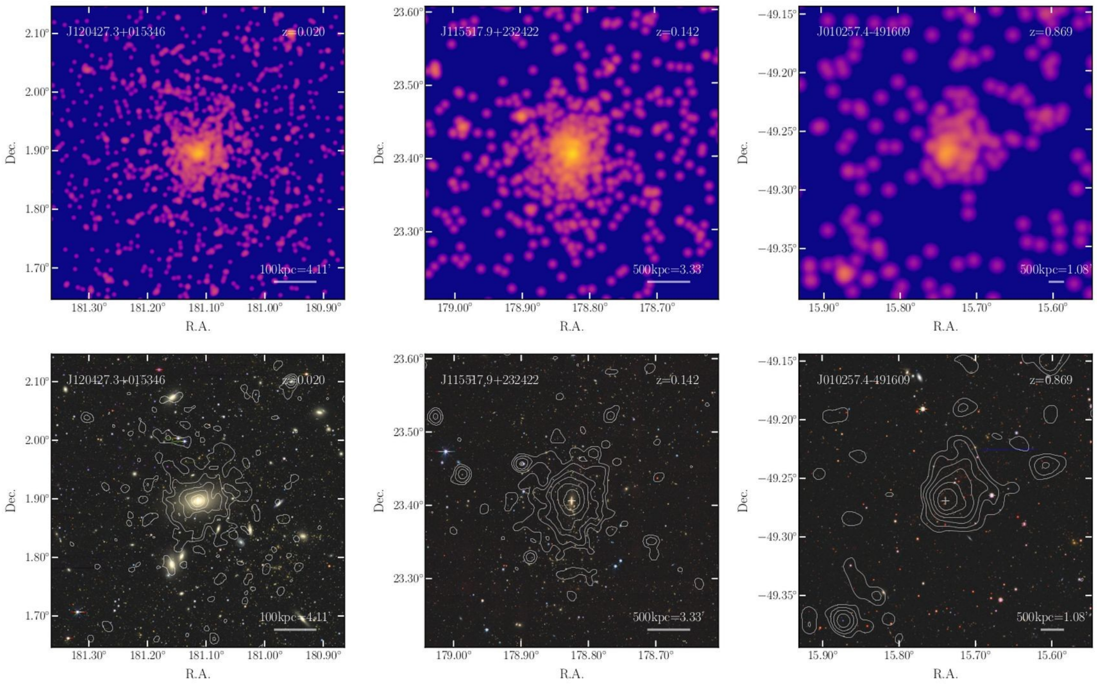

Bulbul et al. (2024)

The eRASS1 galaxy cluster catalog

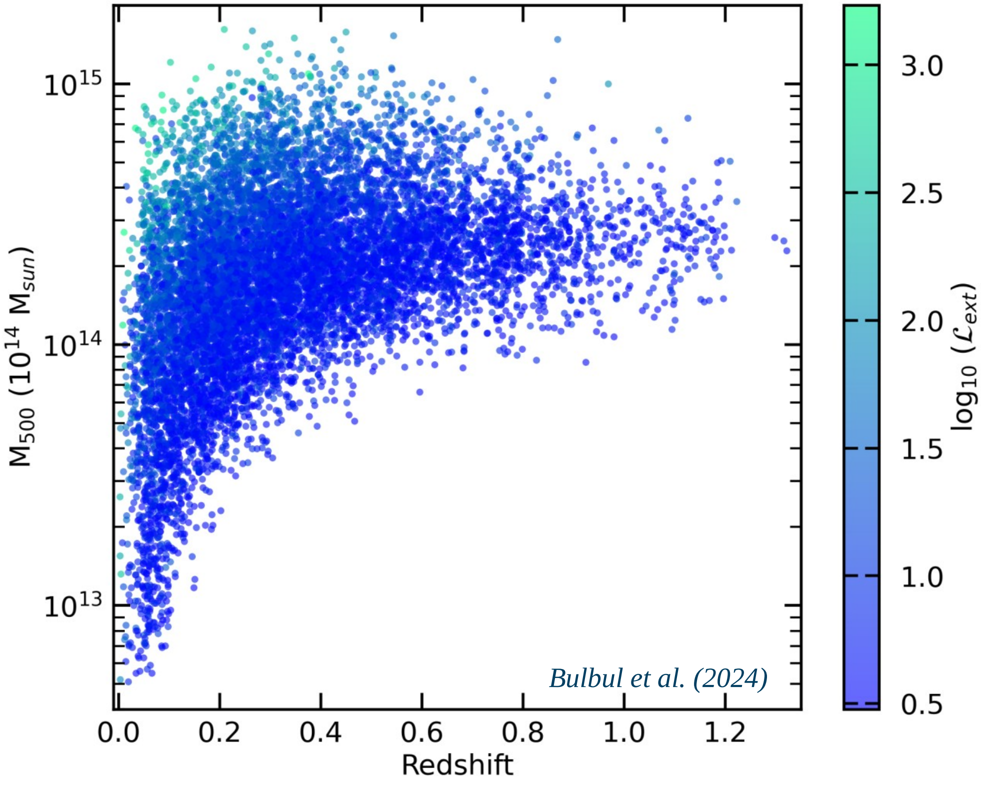

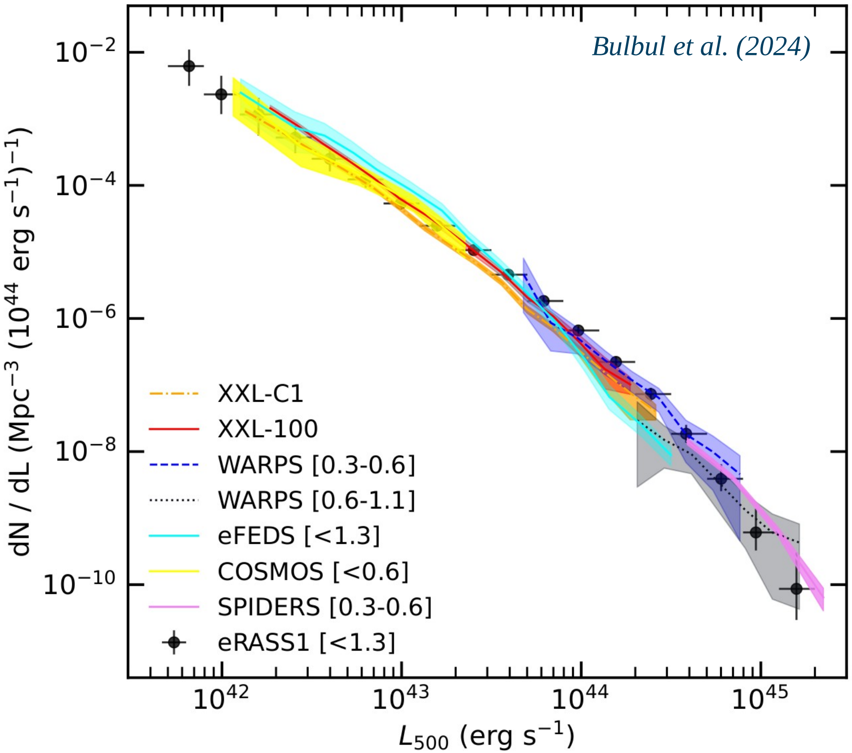

Cosmological constraints from cluster counts: principles of the eRASS1 analysis

- Sub-selection of a least-contaminated sample of clusters
- Calibration of the X-ray count-rate (~flux) and total mass using weak gravitational lensing in overlapping surveys
- Establishment of the sample selection function and residual contamination models
- Forward model: writing up a likelihood linking theoretical predictions to observed distributions
- Testing various models (ΛCDM, νCDM, *w*CDM, ν*w*CDM) and putting constraints on parameters via Bayesian inference
- Blinding/unblinding strategy

Galaxy cluster selection sample: 5259 clusters

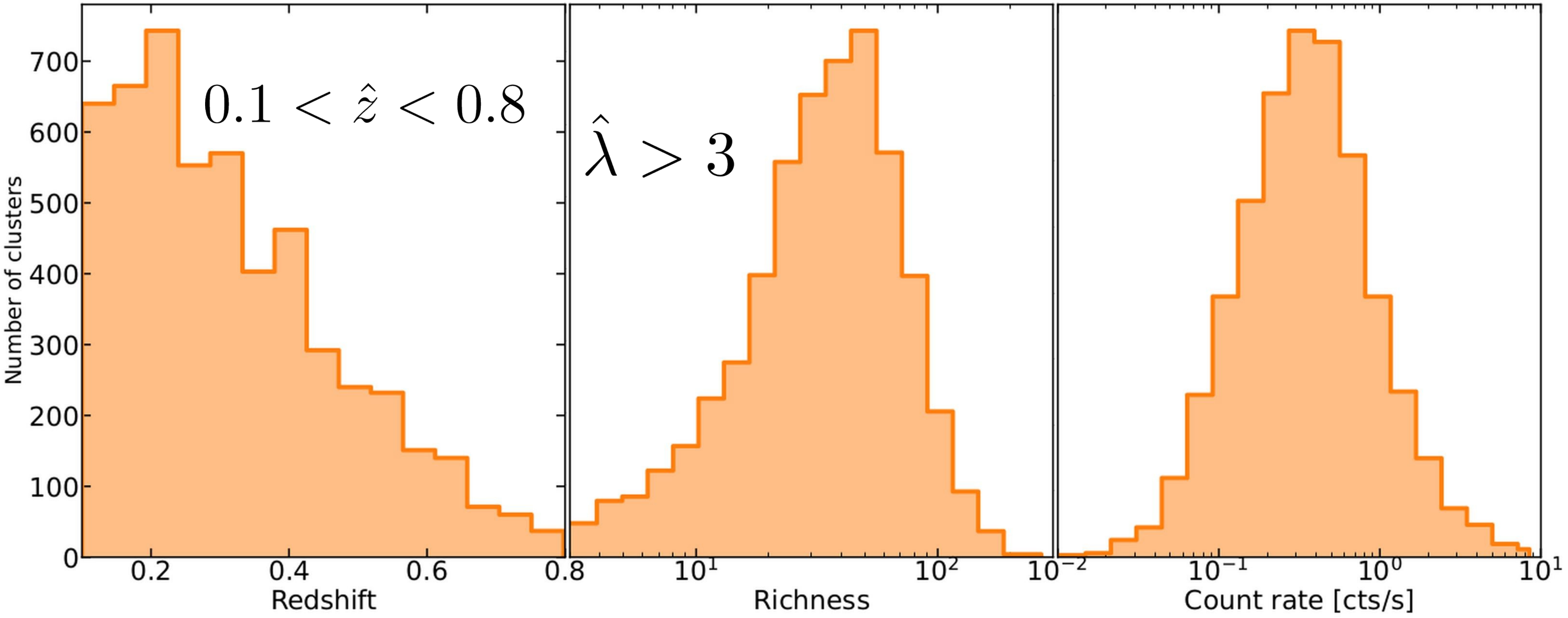

Decomposing the likelihood

$$
\begin{aligned}
\log \mathcal{L} = & \sum_j \log\left(\frac{dN_{tot}}{d\hat{C}_R d\hat{z} d\hat{\lambda} d\hat{\mathcal{H}}_i} P(I|\hat{C}_R, \hat{z}, \hat{\mathcal{H}}_i)\right) \\
& - \int \cdots \int \left[\frac{dN_{tot}}{d\hat{C}_R d\hat{z} d\hat{\lambda} d\hat{\mathcal{H}}_i} P(I|\hat{C}_R, \hat{z}, \hat{\mathcal{H}}_i)\Theta(\hat{\lambda} > 3)\right. \\
& \qquad \left. d\hat{C}_R d\hat{z} d\hat{\lambda} d\hat{\mathcal{H}}_i\right] \\
& + \sum_j \log P(\hat{\lambda}|\hat{C}_R, \hat{z}, \hat{\mathcal{H}}_i, I) \\
& + \sum_{k \text{ with } \hat{g}_t} \log P(\hat{g}_t|\hat{C}_R, \hat{z}, \hat{\mathcal{H}}_i, I)
\end{aligned}
$$

Poisson likelihood for number counts in ‘bins’ of count-rate, redshift, richness, sky position.

j = 5259 clusters, 0.1<z<0.8.

X-ray – optical richness calibration

X-ray – tangential shear calibration

Ghirardini et al. (2024)

Free parameters in the model(s)

Parameter	Units	Description
• Cosmology		
Ω_m	-	Mean matter density at present time
$\log_{10} A_s$	-	Amplitude of the primordial power spectrum
H_0	$\frac{\frac{km}{s}}{Mpc}$	Hubble expansion rate at present time
Ω_b	-	Mean baryon density at present time
n_s	-	Spectra index of the primordial power spectrum
w_0	-	Dark energy equation of state. Fixed to -1 in ΛCDM
$\sum m_\nu$	eV	Summed neutrino masses. Fixed to 0 eV in ΛCDM
• X-ray scaling relation		
A_X	-	Normalization of the $M - C_R$ scaling relation
B_X	-	Mass slope of the $M - C_R$ scaling relation
D_X	-	Luminosity distance evolution of the $M - C_R$ scaling relation
E_X	-	Scale factor evolution of the $M - C_R$ scaling relation
F_X	-	Redshift evolution of the mass slope of the $M - C_R$ scaling relation
G_X	-	Redshift evolution of the normalization of the $M - C_R$ scaling relation
σ_X	-	Intrinsic scatter of the $M - C_R$ scaling relation
• Weak lensing mass calibration		
A_{WL}	-	Scatter in the weak lensing bias from the first principal component
B_{WL}	-	Scatter in the weak lensing bias from the second principal component
C_{WL}	-	Standardize mass slope of the weak lensing bias
D_{WL}	-	Redshift dependent intrinsic scatter in the weak lensing bias
ρ_{M_{WL},C_R}	-	Intrinsic correlation between weak lensing mass and count rate
• Richness mass calibration		
$\log A_\lambda$	-	Normalization of the $M - \lambda$ scaling relation
B_λ	-	Mass slope of the $M - \lambda$ scaling relation
C_λ	-	Redshift evolution of the normalization of the $M - \lambda$ scaling relation
D_λ	-	Redshift evolution of the mass slope of the $M - \lambda$ scaling relation
σ_λ	-	Intrinsic scatter of the $M - \lambda$ scaling relation
ρ_{λ,C_R}	-	Intrinsic correlation between richness and count rate
• Contamination modeling		
f_{AGN}	-	Fraction of AGN contaminants in the extended source sample
f_{RS}	-	Fraction of RS contaminants in the extended source sample
• Redshift uncertainty		
σ_z	-	Relative error on the measured redshift
b_z	-	Systematic bias in our redshift estimate
c_z	-	Fraction of objects for which we measure a shifted redshift
$c_{shift,z}$	-	Amount of redshift shift for c_z fraction of objects

- **'Scaling relations' model a log-normal distribution**
  - Between CR (X-ray flux) and total mass
  - Between weak-lensing mass and total mass
  - Between λ (optical richness) and total mass

Ghirardini et al. (2024)

Decomposing the likelihood – selection function

$$\log \mathcal{L} = \sum_j \log\left(\frac{dN_{tot}}{d\hat{C}_R d\hat{z} d\hat{\lambda} d\hat{\mathcal{H}}_i} P(I|\hat{C}_R, \hat{z}, \hat{\mathcal{H}}_i)\right)$$
$$- \int \cdots \int \left[\frac{dN_{tot}}{d\hat{C}_R d\hat{z} d\hat{\lambda} d\hat{\mathcal{H}}_i} P(I|\hat{C}_R, \hat{z}, \hat{\mathcal{H}}_i) \Theta(\hat{\lambda} > 3) \right. \left. d\hat{C}_R d\hat{z} d\hat{\lambda} d\hat{\mathcal{H}}_i\right]$$
$$+ \sum_j \log P(\hat{\lambda}|\hat{C}_R, \hat{z}, \hat{\mathcal{H}}_i, I)$$
$$+ \sum_{k \text{ with } \hat{g}_t} \log P(\hat{g}_t|\hat{C}_R, \hat{z}, \hat{\mathcal{H}}_i, I)$$

Poisson likelihood for number counts in ‘bins’ of count-rate, redshift, richness, sky position.

j = 5259 clusters, 0.1<z<0.8.

The X-ray selection function model

Ghirardini et al. (2024)

Controlling selection effects through simulations

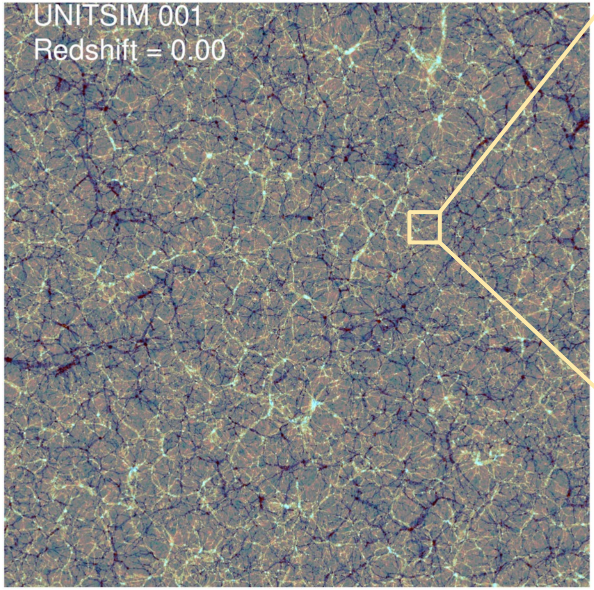

“UNIT1 simulation” Chuang et al. (2019)

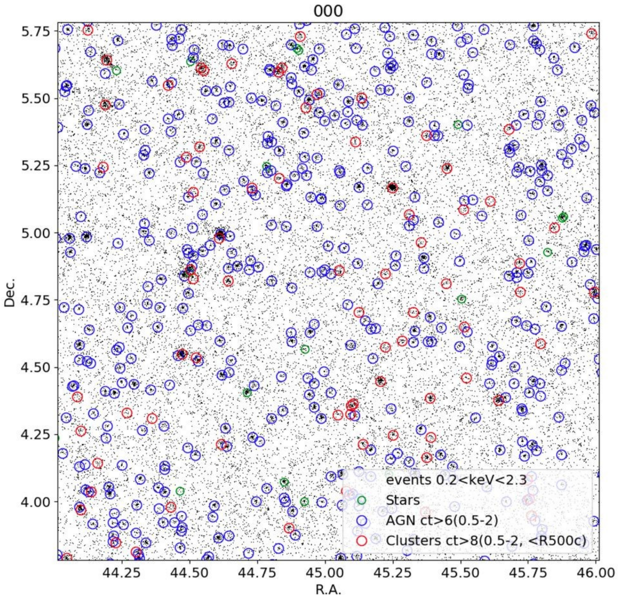

Comparat et al. (2020) ; Seppi et al. (2022)

- **Realistic full-sky simulations**
- All major astro components
- All major instrument features
- Identical processing as real data

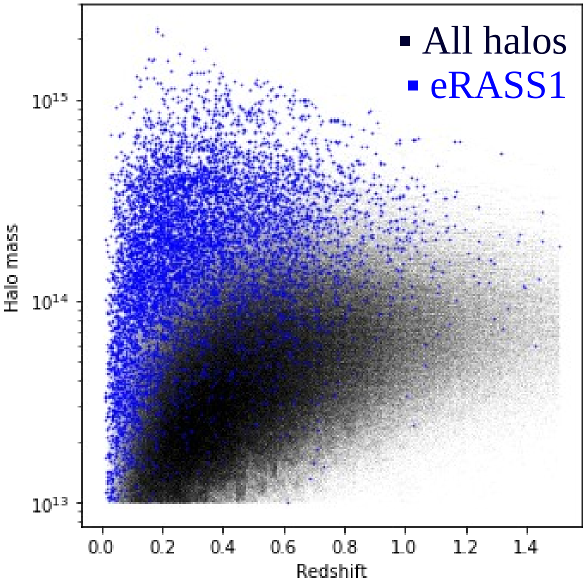

Clerc et al. (2024) – A&A in press

Controlling selection effects through simulations

- **What does selection truly depend on?**
  - Surface brightness features in images
  - Many sources involved: astrophysical, instrumental
  - Complex response of the detection algorithm (eSASS)

- **How to efficiently model selection?**
  - Simulations as training data points
  - Choice of features → necessary compromises with cosmology likelihood complexity

- **How reliable are selection models?**
  - Internal validation on simulations
  - External validation with independent catalogs

Clerc et al. (2024) – A&A in press

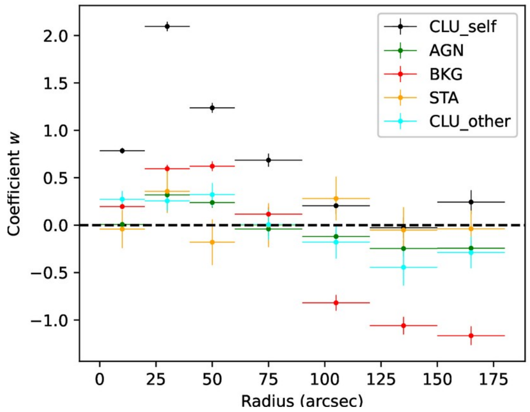

→Detection positively impacted by <1.5' X-ray photons

→Inner-core photons not as helpful as wished (point-source confusion)

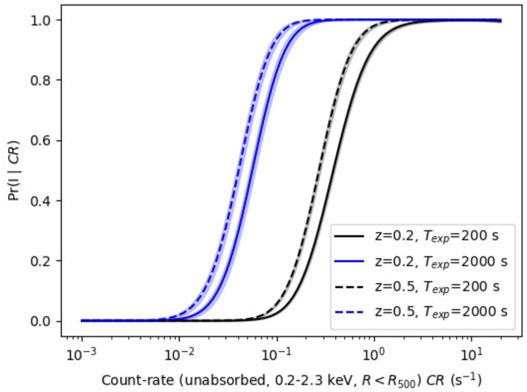

→Final cosmological model involves 5-parameter selection, including X-ray count-rate, redshift, and local sky properties

Validating selection models with external surveys

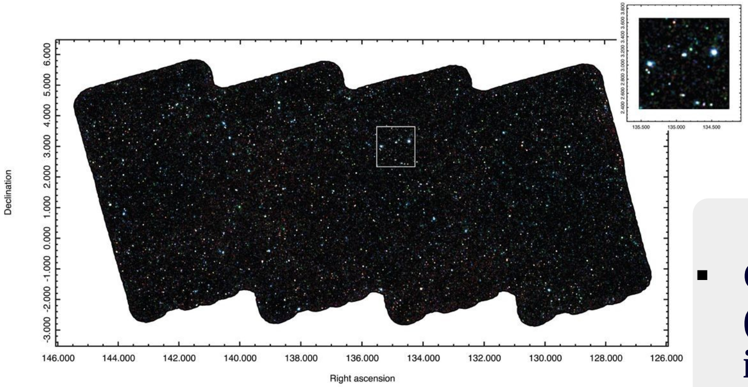

- **Our deep eFEDS survey (150 deg^2) contains lots of identified faint clusters**
  - Test bench for our models

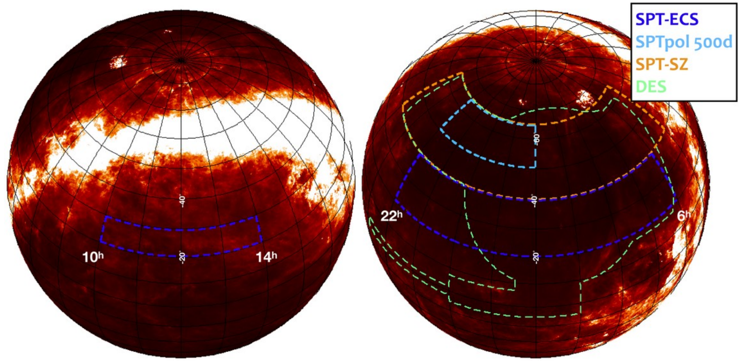

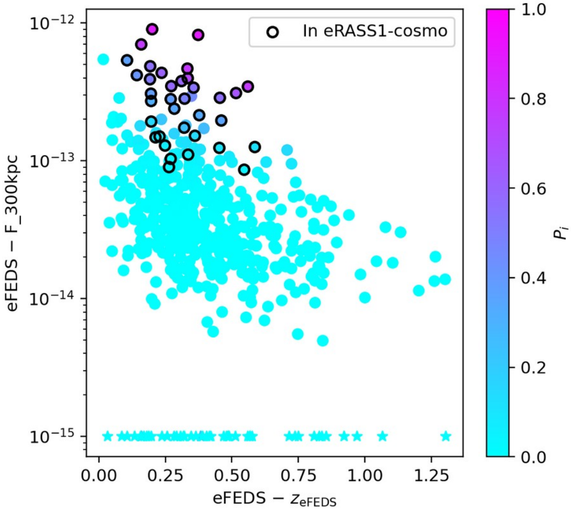

- **The SPT collects massive clusters based on the Sunyaev-Zeldovich effect**
  - Hot gas selection, but different systematics

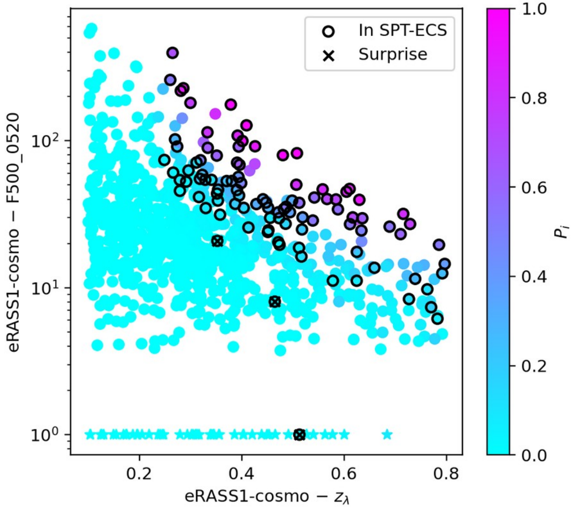

Clerc et al. (2024) – A&A in press

Decomposing the likelihood – WL calibration

$$
\begin{aligned}
\log \mathcal{L} \; = \; & \sum_j \log \left(\frac{dN_{tot}}{d\hat{C}_R d\hat{z} d\hat{\lambda} d\hat{\mathcal{H}}_i} P(I|\hat{C}_R, \hat{z}, \hat{\mathcal{H}}_i) \right) \\
- \; & \int \cdots \int \left[\frac{dN_{tot}}{d\hat{C}_R d\hat{z} d\hat{\lambda} d\hat{\mathcal{H}}_i} P(I|\hat{C}_R, \hat{z}, \hat{\mathcal{H}}_i) \Theta(\hat{\lambda} > 3) \right. \\
& \left. d\hat{C}_R d\hat{z} d\hat{\lambda} d\hat{\mathcal{H}}_i \right] \\
+ \; & \sum_j \log P(\hat{\lambda}|\hat{C}_R, \hat{z}, \hat{\mathcal{H}}_i, I) \\
+ \; & \boxed{\sum_{k \text{ with } \hat{g}_t} \log P(\hat{g}_t|\hat{C}_R, \hat{z}, \hat{\mathcal{H}}_i, I)}
\end{aligned}
$$

X-ray – tangential shear calibration.
k = 2348 clusters with shear information

Ghirardini *et al.* (2024)

Mass calibration through weak gravitational lensing

- **Measurement of light deflections by the cluster gravitational potential:** statistically coherent distortion of randomly oriented background sources
- Strength depends on **integrated surface density** and **geometrical configuration (distance ratios)**

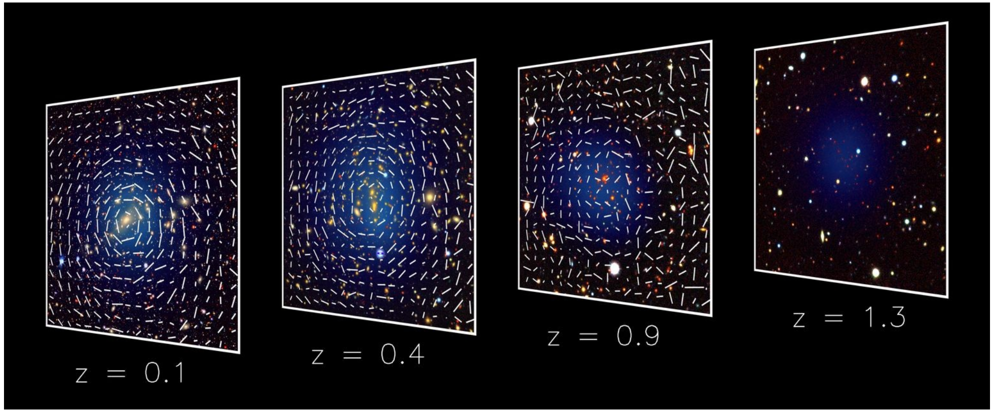

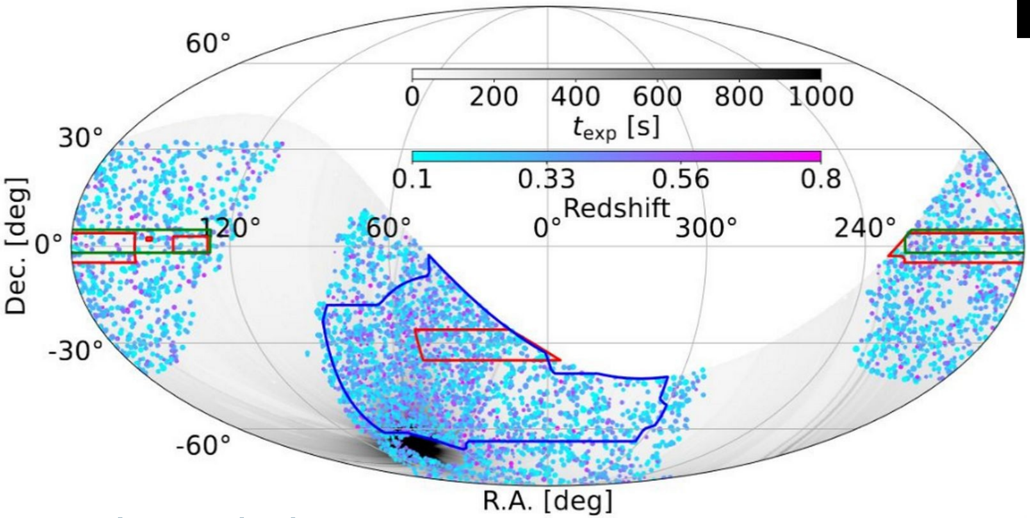

- Consistent use of 3 partially overlapping deep lensing optical surveys: **DES Y3**, **HSC S19A** and **KiDS**

- Observable = reduced shear profiles around eRASS1 galaxy clusters.
  - Direct link to 'weak lensing mass' M_{WL}
  - Model involves calibration of the M_{WL} – M relation

Courtesy S. Grandis, U. Innsbruck

Weak-lensing in the DES Y3 area

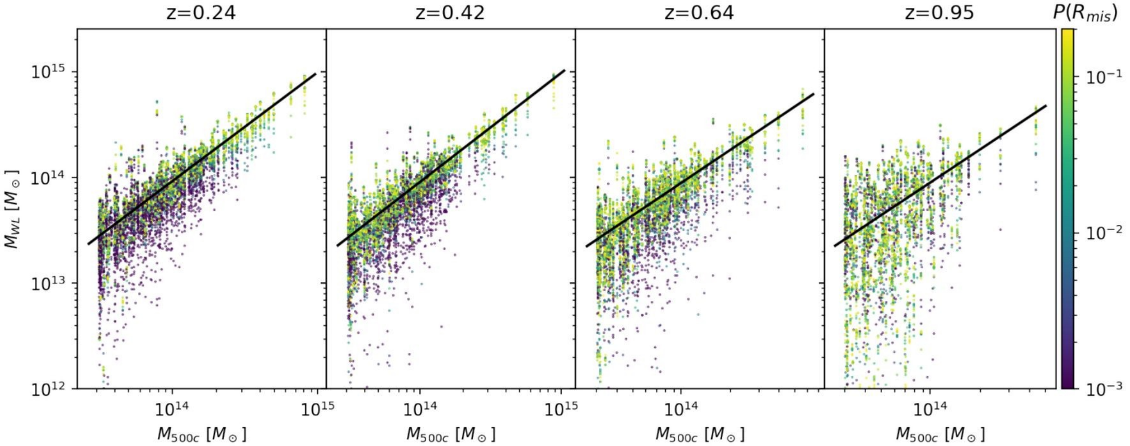

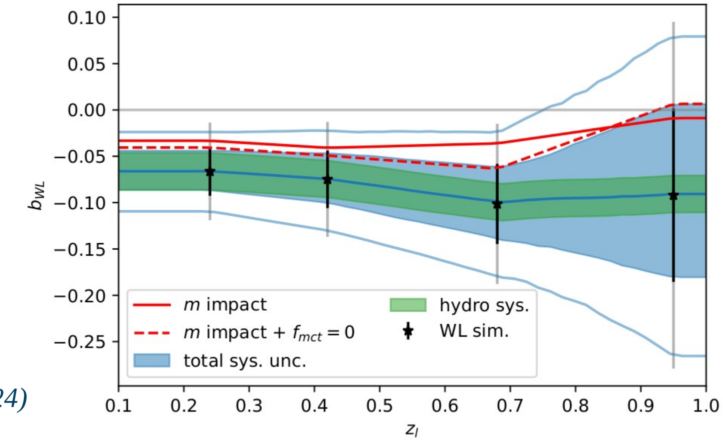

Grandis et al. (2024)

- A **calibrated mass extraction** model from hydrodynamical simulations (Monte-Carlo) provides PDF of shear at fixed WL mass
- Actual WL data over eRASS1 clusters is used to constrain the link between X-ray and total mass.

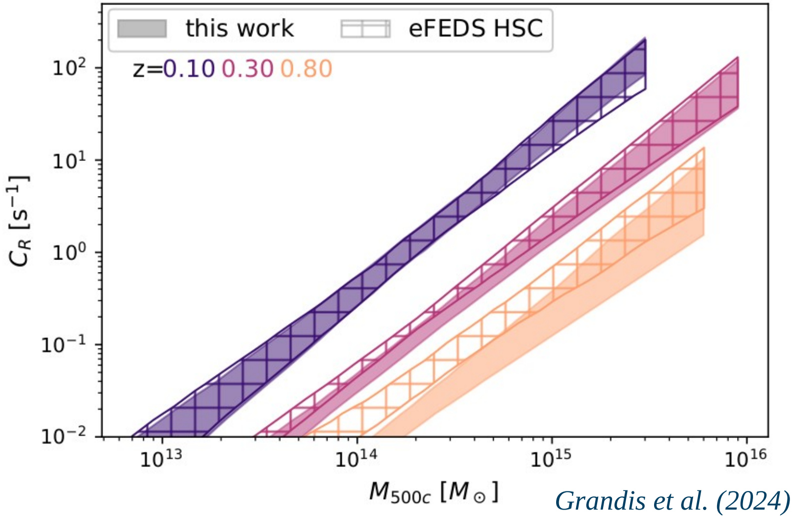

Grandis et al. (2024)

Consistency between DES, HSC and KiDS lensing

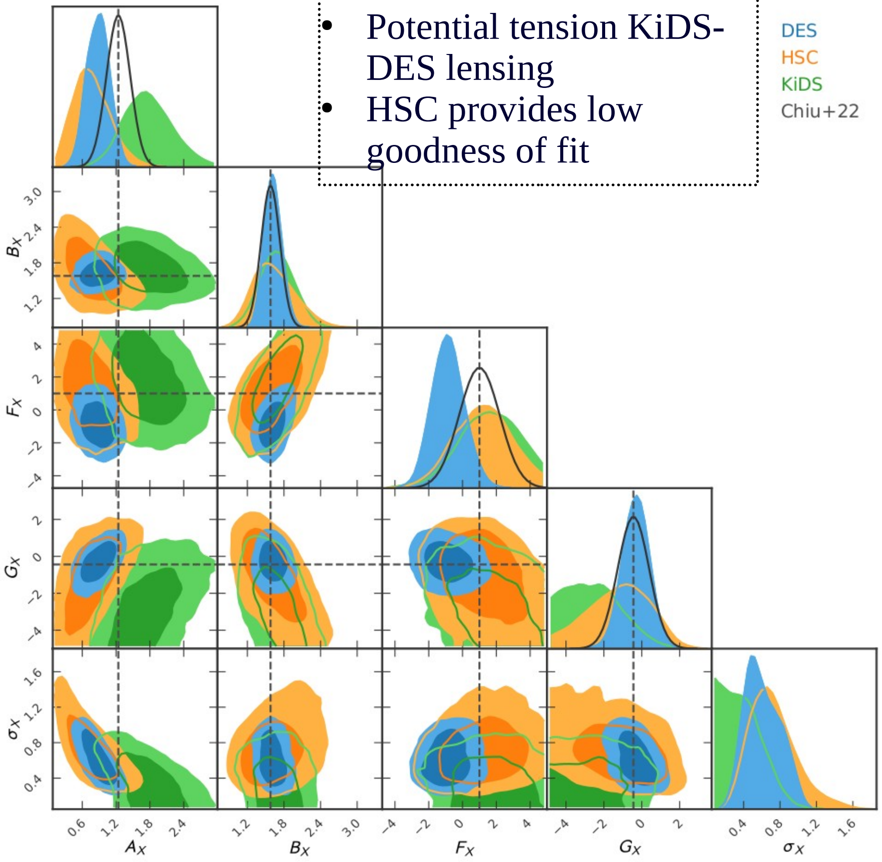

- Potential tension KiDS-DES lensing
- HSC provides low goodness of fit

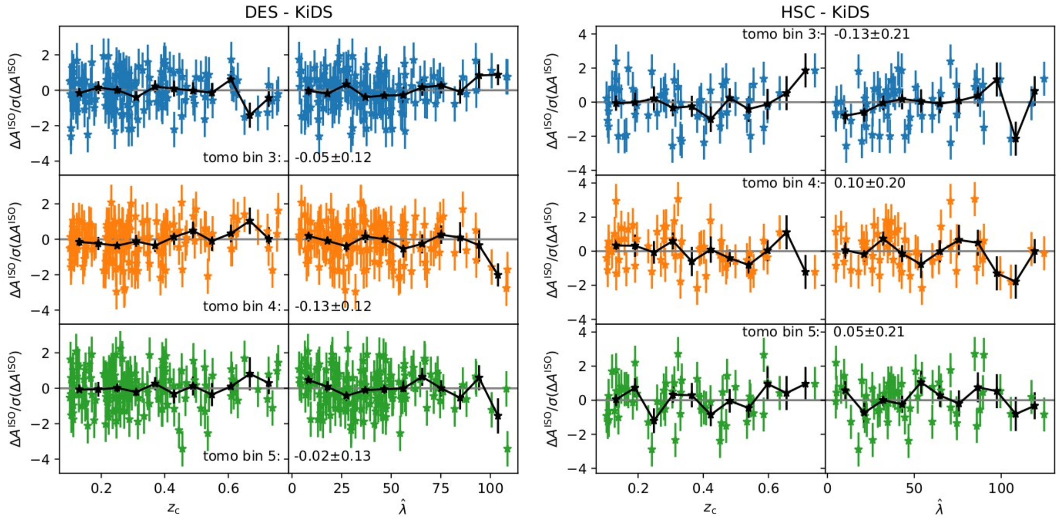

- Comparisons at the population level (i.e. consistency of inferred X-lensing scaling relations)
- Direct comparison in the overlapping sky areas

Kleinebreil et al. (2024)

Constraints on ΛCDM from eRASS1

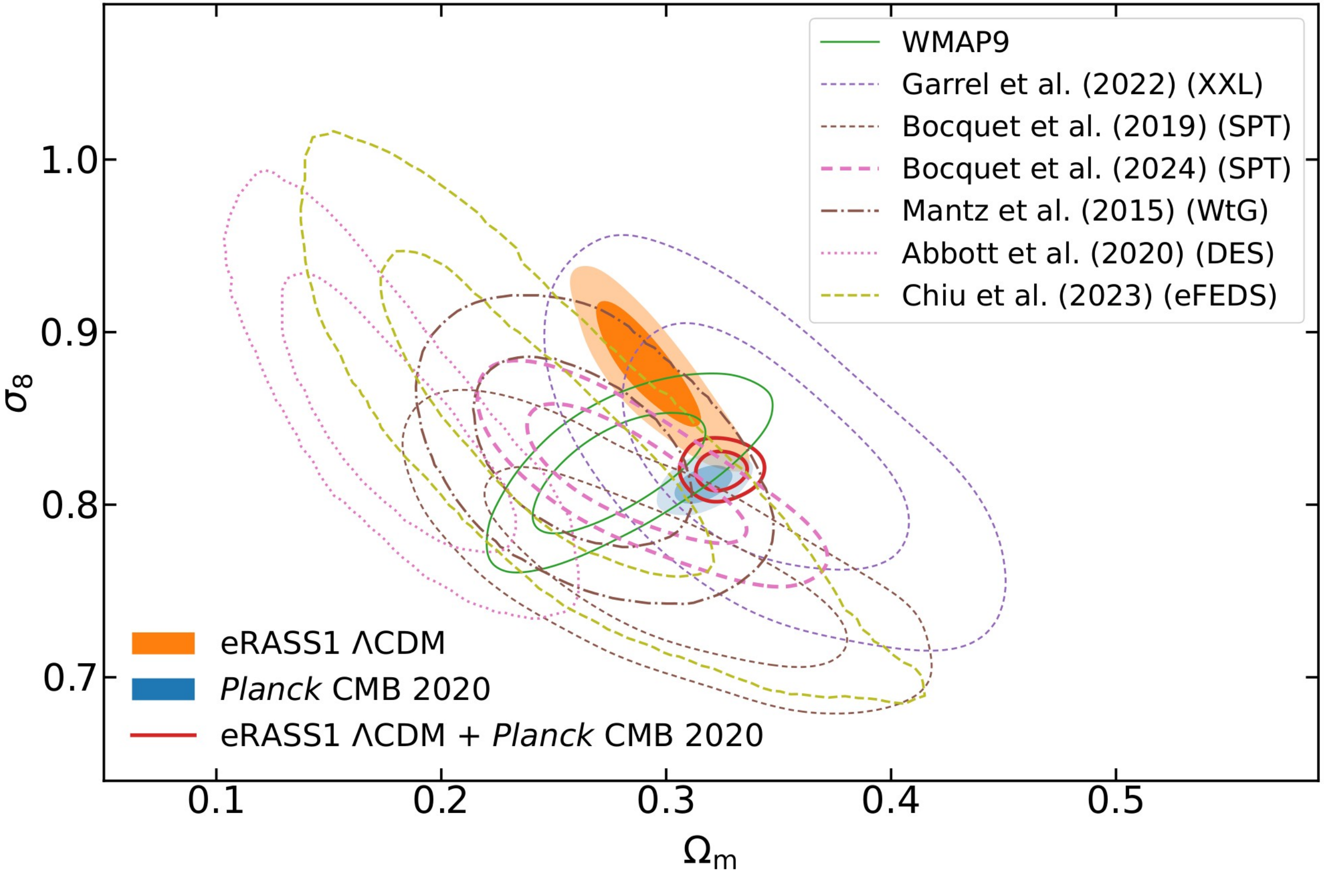

- **From eRASS1 clusters:**

$$\Omega_m = 0.29^{+0.01}_{-0.02}$$
$$\sigma_8 = 0.88 \pm 0.02$$
$$S_8 = 0.86 \pm 0.01$$

- **With Planck CMB 2020:**

$$\Omega_m = 0.32 \pm 0.01$$
$$\sigma_8 = 0.82 \pm 0.01$$
$$S_8 = 0.85 \pm 0.01$$

Ghirardini, Bulbul, Artis, NC et al. 2024

Constraints on ΛCDM from eRASS1

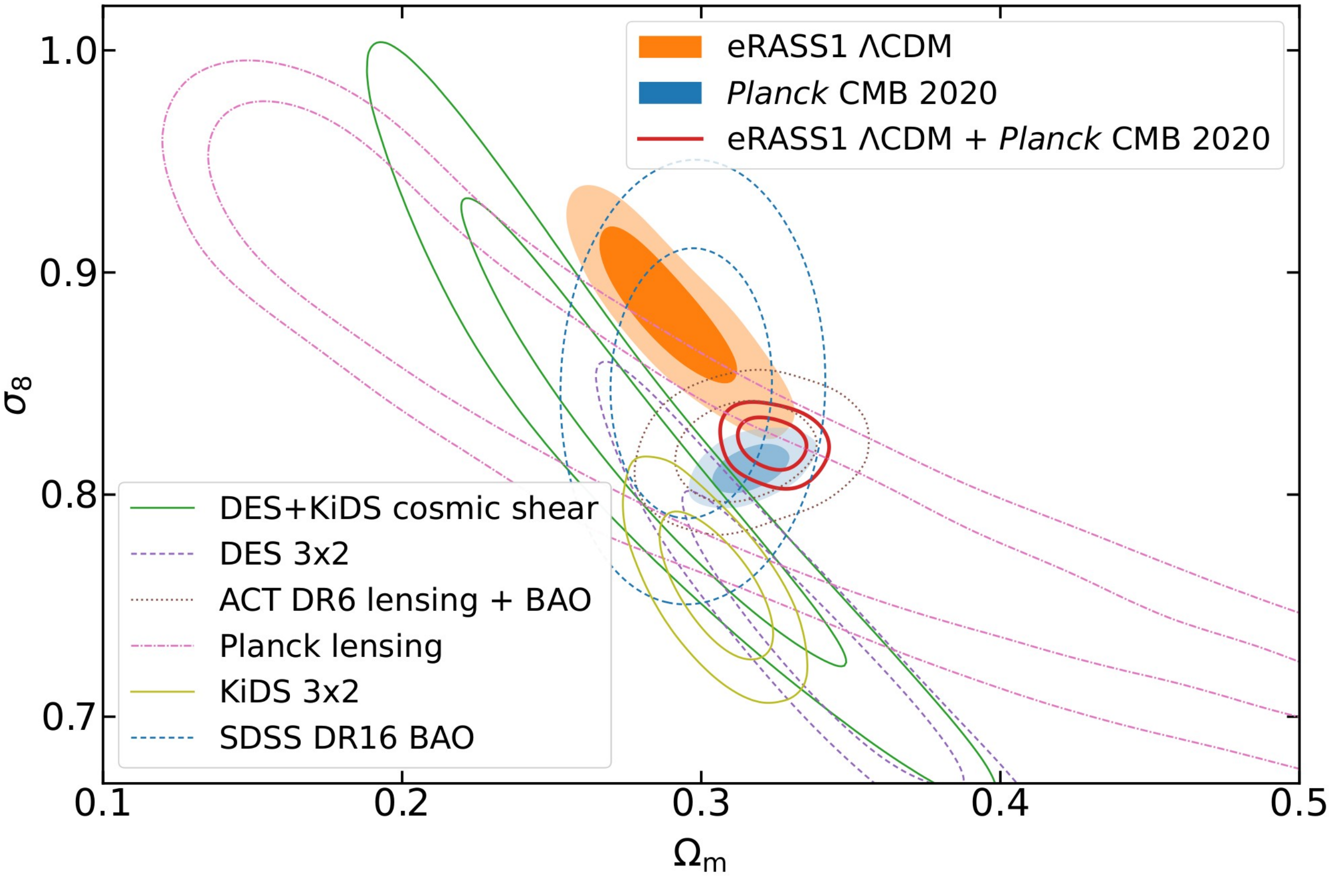

- **From eRASS1 clusters:**

$$\Omega_m = 0.29^{+0.01}_{-0.02}$$
$$\sigma_8 = 0.88 \pm 0.02$$
$$S_8 = 0.86 \pm 0.01$$

- **With Planck CMB 2020:**

$$\Omega_m = 0.32 \pm 0.01$$
$$\sigma_8 = 0.82 \pm 0.01$$
$$S_8 = 0.85 \pm 0.01$$

Ghirardini, Bulbul, Artis, NC et al. 2024

ΛCDM constraints shedding light on the “S_8 tension”

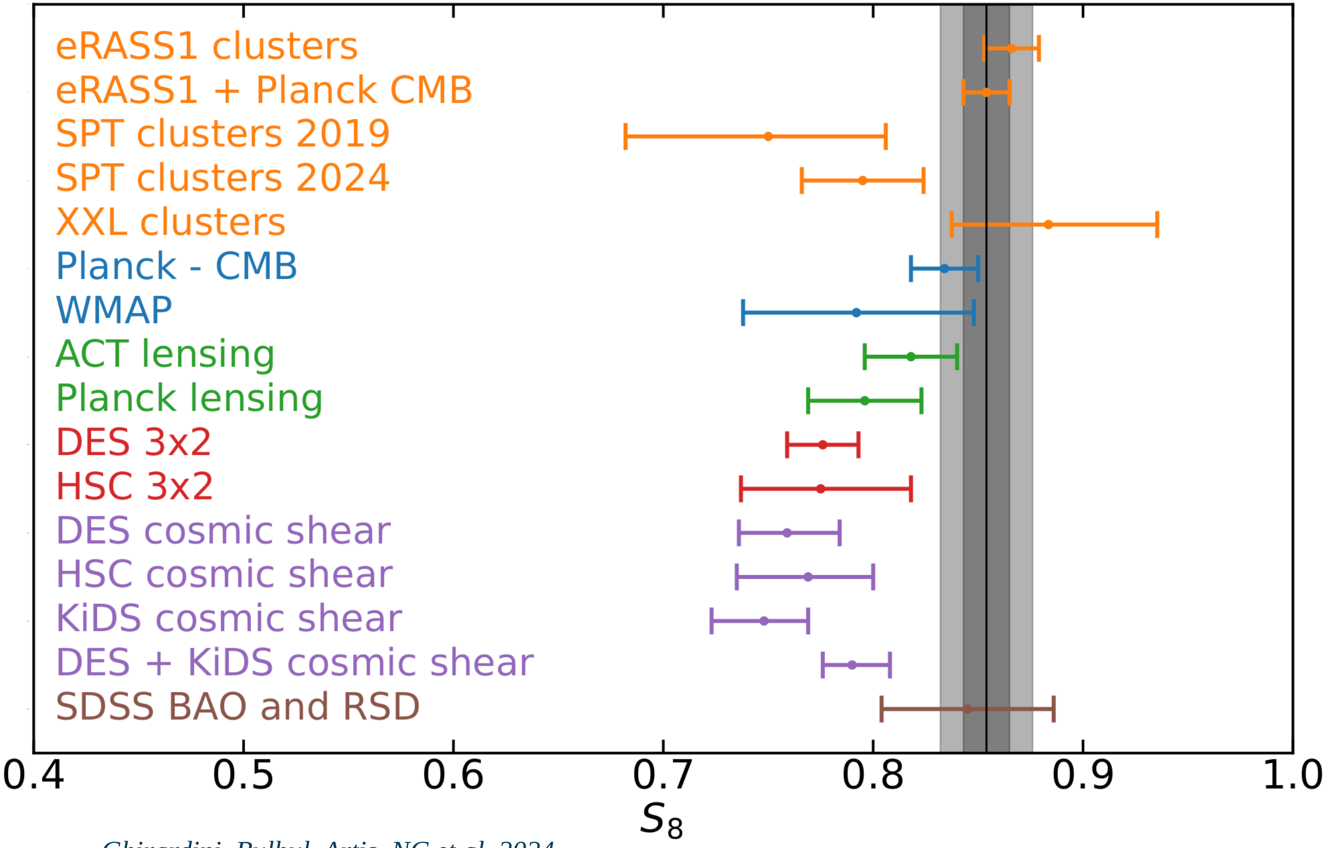

Ghirardini, Bulbul, Artis, NC et al. 2024

νCDM: alleviating for non-zero neutrino masses

- **Massive relic neutrinos impact the growth of massive clusters**

  - Impact the expansion rate H(z), prevent small-mass halo clustering due to their large free-streaming lengths
  - Shift the matter-radiation equality

- **Stringent upper limit constraints**

  - $\Sigma m_\nu < 0.43$ eV (95% C.L.) [eRASS1 alone]
  - $\Sigma m_\nu < 0.14$ eV (95% C.L.) [+CMB]

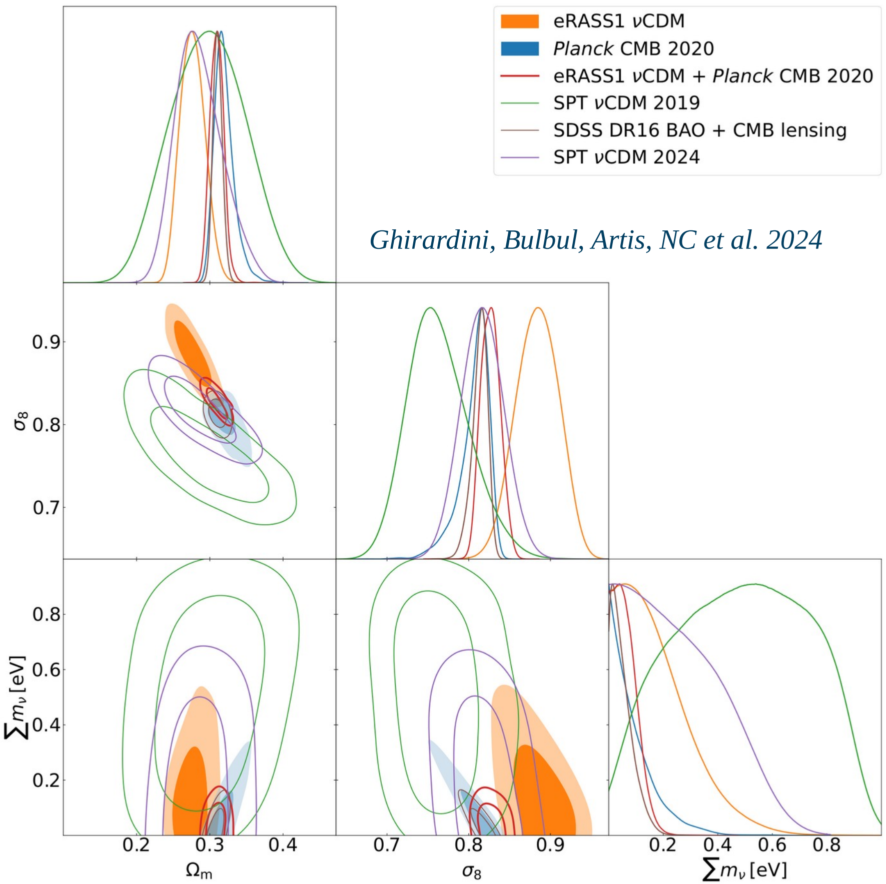

Ghirardini, Bulbul, Artis, NC et al. 2024

wCDM: exploring the dark energy equation of state in the form P=$w\rho$

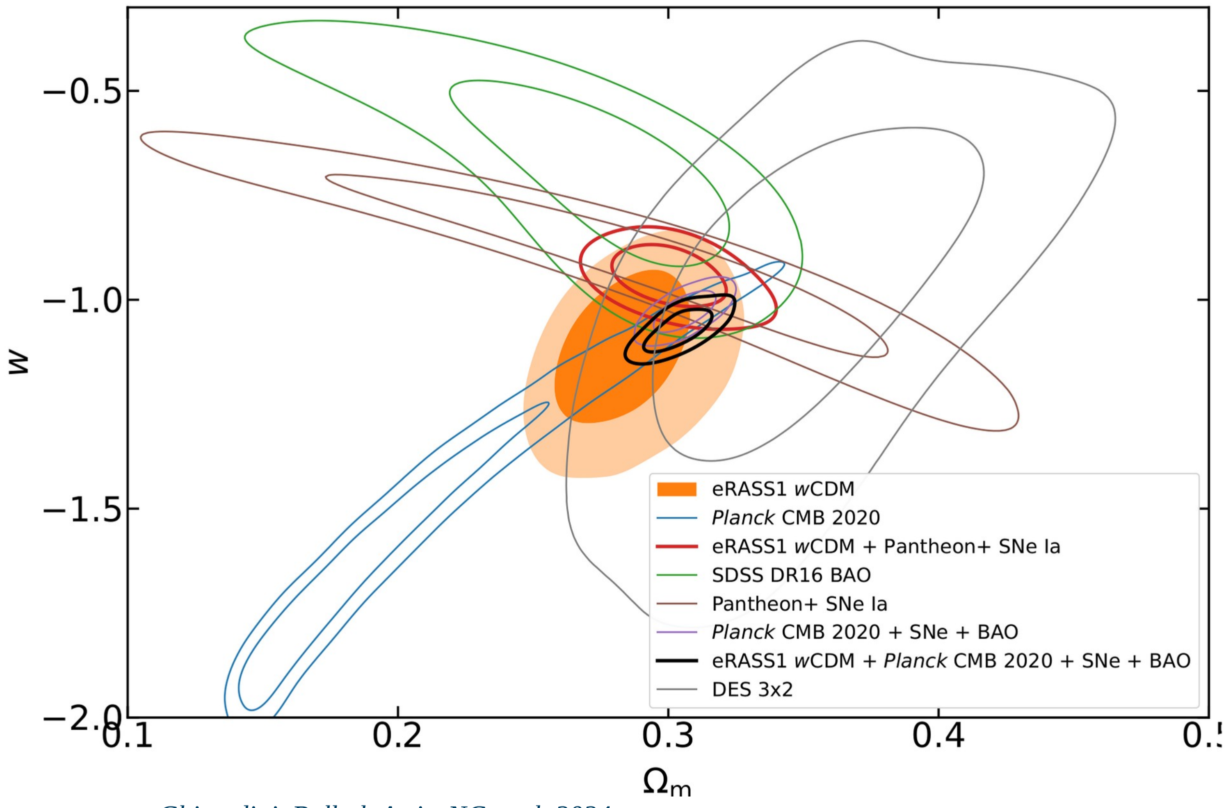

Ghirardini, Bulbul, Artis, NC et al. 2024

- **From eRASS1 clusters:**

$$\Omega_m = 0.28 \pm 0.02$$
$$\sigma_8 = 0.88 \pm 0.02$$
$$S_8 = 0.86 \pm 0.02$$
$$w = -1.12 \pm 0.12$$

- **With Pantheon SneIa:**

$$\Omega_m = 0.30 \pm 0.01$$
$$\sigma_8 = 0.87 \pm 0.02$$
$$S_8 = 0.87 \pm 0.01$$
$$w = -0.95^{+0.05}_{-0.04}$$

- **W/ Pantheon+BAO+CMB:**

$$\Omega_m = 0.31 \pm 0.01$$
$$\sigma_8 = 0.84 \pm 0.01$$
$$S_8 = 0.85 \pm 0.01$$
$$w = -1.06 \pm 0.03$$

νwCDM: most extensive model tested

- **From eRASS1 clusters:**

$$\Omega_m = 0.27 \pm 0.02$$
$$\sigma_8 = 0.89 \pm 0.03$$
$$S_8 = 0.84 \pm 0.02$$
$$w = -1.11 \pm 0.14$$
$$\sum m_\nu < 0.44 \text{ eV} \quad (95\% \text{ CL})$$

- **With Planck CMB 2016+lensing+BAO:**

$$\Omega_m = 0.29 \pm 0.01$$
$$\sigma_8 = 0.85 \pm 0.02$$
$$S_8 = 0.83 \pm 0.01$$
$$w = -1.15 \pm 0.10$$
$$\sum m_\nu < 0.37 \text{ eV} \quad (95\% \text{ CL})$$

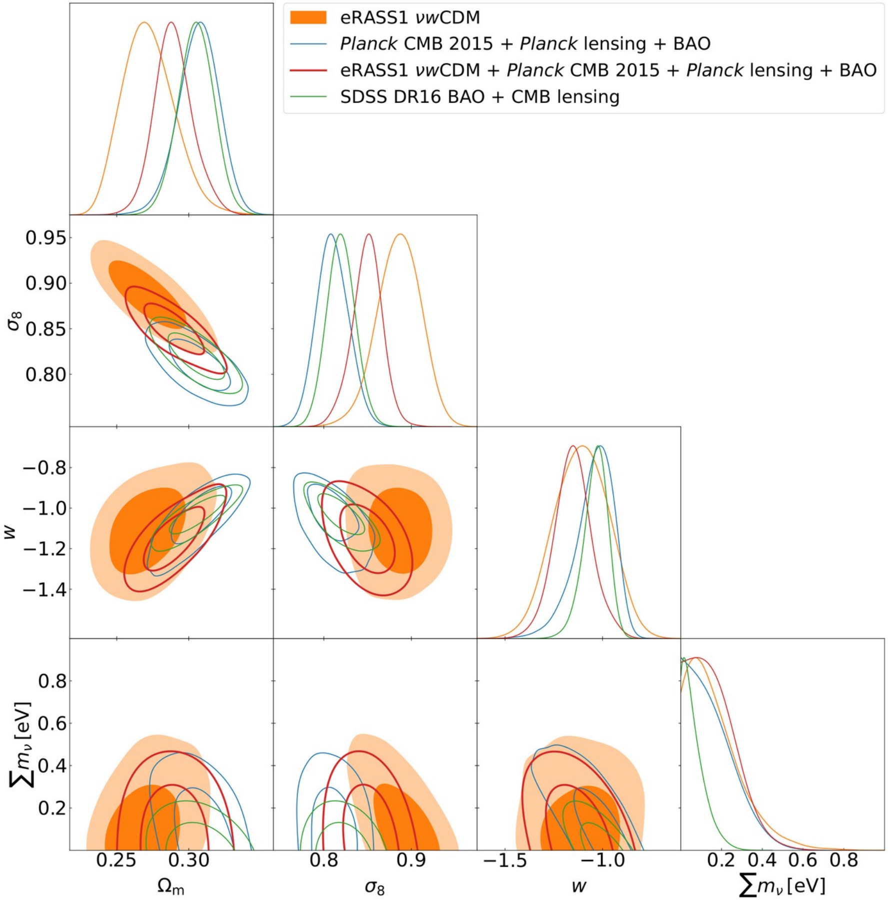

Ghirardini, Bulbul, Artis, NC et al. 2024

Perspectives: complementary eRASS1 cluster cosmology studies and deeper eRASS:n surveys

- **eRASS1 clusters trace the LSS**
  - 2-point correlation function (w/ mass)
  - Superclusters in the cosmic web
  - Tests of modified gravity f(R)

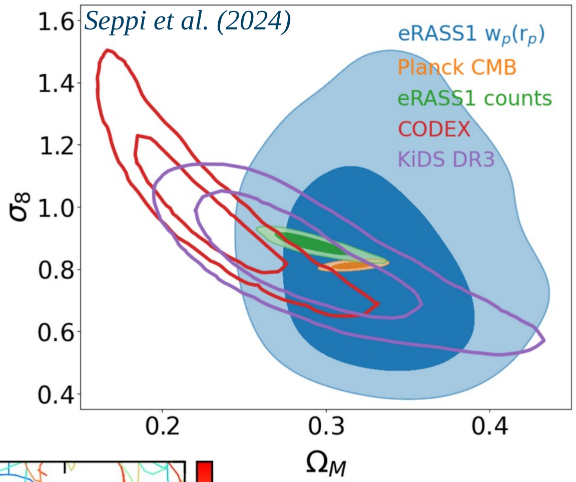

Seppi et al. (2024)

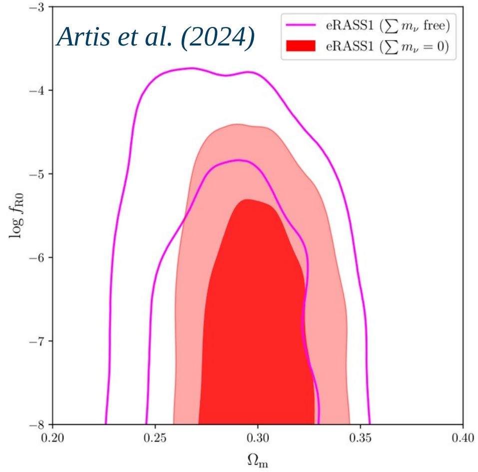

Artis et al. (2024)

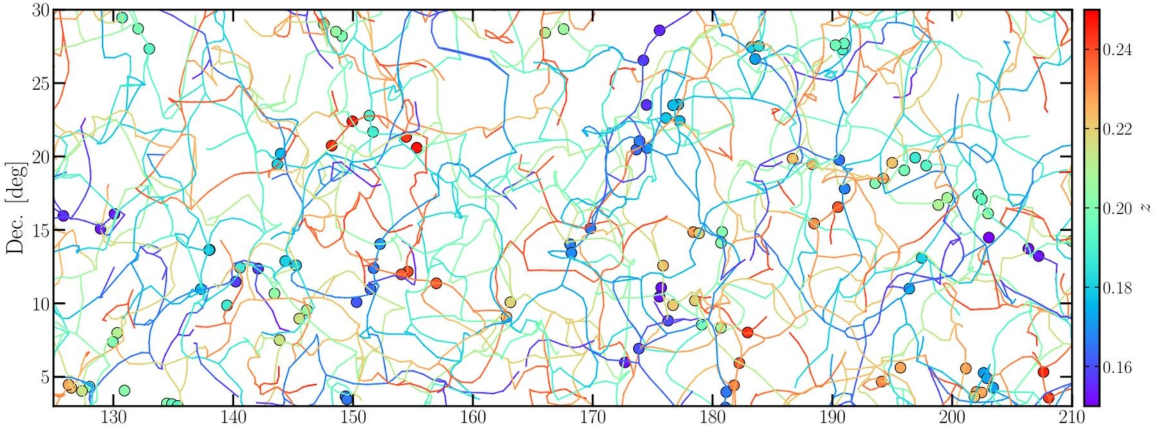

Liu et al. (2024)

- **eRASS1 is just 6 months of data among the 2 years of survey**
  - Higher-z, lower-M datasets
  - Better individual characterization of cluster fluxes, temperatures, masses

Conclusions

- Presented cosmological constraints from the abundance of X-ray selected galaxy clusters in the first eROSITA all-sky survey Western hemisphere with monitored control on selection effects
- Optical data to obtain redshifts, richness and important weak-lensing mass to X-ray observable calibration
- Not confirming the S_8 tension between late- and early-time probes
- Combining with Planck CMB, tightest upper limit on summed neutrinos mass to date, exclusion of the inverted hierarchy at 93% C.L.
- Dark energy equation of state compatible with cosmological constant (w = -1) with 10% precision
- A factor 5 to 9 improvement in the "figure of merit" over previously published galaxy cluster abundance cosmology results
- **Cluster abundances are a reliable experiment in precision cosmology.**

Thank you!